



ORIGINAL ARTICLE

Galectin 3-binding protein (LGALS3BP) depletion attenuates hepatic fibrosis by reducing transforming growth factor- β 1 (TGF- β 1) availability and inhibits hepatocarcinogenesis

Dae-Hwan Kim^{1,2,3,4} | Minjeong Sung^{1,2,3,4,5} | Myong-Suk Park^{1,2,3,4} |
 Eun-Gene Sun^{1,2,4} | Sumin Yoon⁶ | Kyung Hyun Yoo⁶  |
 Kamalakannan Radhakrishnan⁷ | Sung Yun Jung⁸ | Woo-Kyun Bae^{1,2,3,4,5} |
 Sang-Hee Cho^{1,2,3,4} | Ik-Joo Chung^{1,2,3,4} 

¹Department of Internal Medicine, Division of Hematology and Oncology, Chonnam National University Medical School, Hwasun, South Korea

²Department of Internal Medicine, Division of Hematology and Oncology, Chonnam National University Hwasun Hospital, Hwasun, South Korea

³Combinatorial Tumor Immunotherapy MRC Center, Chonnam National University Medical School, Hwasun, South Korea

⁴National Immunotherapy Innovation Center, Hwasun, South Korea

⁵BioMedical Sciences Graduate Program, Chonnam National University, Hwasun, South Korea

⁶Department of Biological Science, Sookmyung Women's University, Seoul, South Korea

⁷Clinical Vaccine R&D Center, Chonnam National University, Hwasun, South Korea

⁸Department of Biochemistry and Molecular Pharmacology, Baylor College of Medicine, Houston, Texas, USA

Correspondence

Ik-Joo Chung, Sang-Hee Cho and
 Woo-Kyun Bae, 264, Seoyang-ro,
 Hwasun-eup, Hwasun-gun, Jeollanam-do,
 58128, South Korea.

Abstract

Background: Increased Galectin 3-binding protein (LGALS3BP) serum levels have been used to assess hepatic fibrosis stages and the severity of hepatocellular carcinoma (HCC). Considering the crucial role of transforming growth factor- β 1

List of Abbreviations: ACTA2, actin alpha 2, smooth muscle 2; ATAC-seq, assay for transposase-accessible chromatin with sequencing; CAF, cancer-associated fibroblast; cDNA, complementary DNA; ChIP, chromatin immunoprecipitation; CNUHH, Chonnam National University Hwasun Hospital; COL1A1, collagen type I alpha 1; CM, culture medium; CRISPR, clustered regularly interspaced short palindromic repeats; DAPI, 4',6-diamidino-2-phenylindole; DEG, differentially expressed gene; DEN, diethylnitrosamine; ECM, extracellular matrix; ELISA, enzyme-linked immunosorbent assay; F-actin, filamentous actin; H&E, hematoxylin and eosin; HBV, hepatitis B virus; HCC, hepatocellular carcinoma; HCV, hepatitis C virus; HFD, high-fat diet; IFN, interferon; IP, intraperitoneally; IRF7, interferon regulatory factor 7; ITG, integrin; JunB, JunB proto-oncogene; KI, knockin; KO, knockout; LC-MS/MS, liquid chromatography-tandem mass spectrometry; LGALS3BP, galectin 3-binding protein; LIF, LIF interleukin 6 family cytokine; MMP, matrix metalloproteinase; MT, Masson's trichrome; MASH, metabolic dysfunction-associated steatohepatitis; p-FAK, phosphorylated focal adhesion kinase; PDGFB, platelet-derived growth factor subunit B; PPI, protein-protein interaction; qRT-PCR, quantitative reverse transcription-polymerase chain reaction; RE, response element; rLGALS3BP, recombinant LGALS3BP; rTGF- β 1, recombinant TGF- β 1; RNA-seq, RNA sequencing; SEM, standard error of the mean; SERPINE1, serpin family E member 1; siRNA, short-interfering RNA; SMAD2, SMAD family member 2; SPPI, secreted phosphoprotein 1; TCGA, The Cancer Genome Atlas; TGF- β 1, transforming growth factor- β 1; VCAM1, vascular cell adhesion molecule 1.

Dae-Hwan Kim and Minjeong Sung contributed equally to this work.

This is an open access article under the terms of the [Creative Commons Attribution-NonCommercial-NoDerivs](https://creativecommons.org/licenses/by-nc-nd/4.0/) License, which permits use and distribution in any medium, provided the original work is properly cited, the use is non-commercial and no modifications or adaptations are made.

© 2024 The Author(s). *Cancer Communications* published by John Wiley & Sons Australia, Ltd on behalf of Sun Yat-sen University Cancer Center.

Email: ijchung@jnu.ac.kr,
shcho@jnu.ac.kr and
drwookyun@jnu.ac.kr

Funding information

Bio & Medical Technology Development
 Program of the National Research
 Foundation, Grant/Award Numbers:
 NRF-2020M3A9G3080281,
 NRF-2020R1A5A2031185; Korean
 Government

(TGF- β 1) in the emergence of these diseases, the present study tested the hypothesis that LGALS3BP regulates the TGF- β 1 signaling pathway.

Methods: The expression levels of *LGALS3BP* and *TGFB1* were analyzed in patients with metabolic dysfunction-associated steatohepatitis (MASH) and HCC. Multiple omics techniques, such as RNA-sequencing, transposase-accessible chromatin-sequencing assay, and liquid chromatography-tandem mass spectrometry proteomics, were used to identify the regulatory mechanisms for the LGALS3BP-TGF- β 1 axis. The effects of altered TGF- β 1 signaling by LGALS3BP were investigated in conditional *LGALS3BP*-knockin and *LGALS3BP*-knockout mice.

Results: In patients with MASH and HCC, the levels of *LGALS3BP* and *TGFB1* exhibited positive correlations. Stimulation of LGALS3BP by the inflammatory cytokine interferon α in HCC cells or ectopic overexpression of LGALS3BP in hepatocytes promoted the expression levels of TGFB1. Aggravated fibrosis was observed in the livers of hepatocyte-specific *LGALS3BP*-knockin mice, with increased TGFB1 levels. LGALS3BP directly bound to and assembled integrin α V, an integral mediator required for releasing active TGF- β 1 from extracellular latent complex with the rearranged F-actin cytoskeleton. The released TGF- β 1 activated JunB transcription factor, which in turn promoted the TGF- β 1 positive feedback loop. *LGALS3BP* deletion in the hepatocytes downregulated TGF- β 1 signaling and CCl₄ induced fibrosis. Moreover, *LGALS3BP* depletion hindered hepatocarcinogenesis by limiting the availability of fibrogenic TGF- β 1.

Conclusion: LGALS3BP plays a crucial role in hepatic fibrosis and carcinogenesis by controlling the TGF- β 1 signaling pathway, making it a promising therapeutic target in TGF- β 1-related diseases.

KEYWORDS

F-actin, FAK, hepatic carcinogenesis, Integrin α V, Interferon α , JunB, LGALS3BP, metabolic dysfunction-associated steatohepatitis, tensile force, TGF- β 1

1 | BACKGROUND

Hepatocellular carcinoma (HCC) is the most prevalent form of primary liver cancer and usually emerges in the context of chronic inflammation. The primary causes of persistent hepatic inflammation include long-term infections with hepatitis B virus (HBV) and hepatitis C virus (HCV), and sterile inflammation caused by alcohol abuse and metabolic disorders. The excessive inflammation results in the constant death of parenchymal cells and activation of non-parenchymal cells, which ultimately contribute to the development of hepatic fibrosis, cirrhosis, and HCC [1–3].

Galectin 3-binding protein (LGALS3BP), also refers to as Gal3-BP, 90K, CyCAP, and Mac2-BP, is a secreted multifunctional glycoprotein whose expression is stimulated under inflammatory conditions, particularly by

type I interferons (IFNs) [4, 5]. LGALS3BP has been studied for its regulatory role in innate immunity [4–6], multiorgan fibrosis [7–9], and carcinogenesis [5, 10–13]. Increased LGALS3BP levels in individuals with viral infections, including HBV [14, 15] and HCV [16, 17], and more recently, severe acute respiratory syndrome coronavirus 2 infections, have been implicated in the regulation of antiviral immune responses [18]. Serum levels of LGALS3BP and its disease-specific N-glycosylation have been used as biomarkers for evaluating the stages of hepatic [19] and pulmonary fibrosis [7] and other fibrotic liver-associated diseases [7, 20, 21]. The prognostic value of LGALS3BP has also been investigated in patients with HCC [22, 23].

Transforming growth factor beta (TGF- β) plays a crucial role in chronic inflammation-related diseases [24, 25]. TGF- β signaling generally inhibits normal epithelial, endothelial, and immune cell proliferation and promotes

the differentiation of fibroblast cell lineages that deposit extracellular matrix (ECM) components [24–26]. When parenchymal cells are infected by viruses or are undergoing necrosis, they signal neighboring cells to establish an inflammatory environment, and TGF- β 1 plays an essential role in this process [24–27]. Hepatic tumor cells are formed primarily through the transformation of mature hepatocytes, which can bypass the anti-proliferation mechanisms of the TGF- β signaling pathway and exploit the suppression of immune cells in the tumor microenvironment to their advantage [27]. The mammalian genome encodes three TGF- β isoforms (TGF- β 1, TGF- β 2, and TGF- β 3), with TGF- β 1 being the principal isoform involved in fibrosis. Latent TGF- β 1 homodimers are stored in the ECM, along with accessory proteins, until an appropriate stimulus is received [28–30]. However, the mechanism underlying the initial pulling force to release active TGF- β 1 remains unclear.

Given the role of type I IFN-induced LGALS3BP in diagnosing liver fibrosis and HCC and the association between TGF- β 1 and fibrogenic diseases and poor clinical outcomes in patients with HCC, we hypothesized that LGALS3BP would directly regulate the TGF- β 1 signaling pathway under IFN- α -primed inflammatory conditions. To test the hypothesis, multi-omics strategies were employed to explore the molecular basis of the LGALS3BP-TGF- β 1 axis, and relevant mouse models of fibrogenic disease and HCC with hepatocyte-specific overexpression or systemic depletion of *LGALS3BP* were examined.

2 | MATERIALS AND METHODS

2.1 | Public database analysis

The Cancer Genome Atlas (TCGA, <http://www.cbioportal.org>, Liver Hepatocellular Carcinoma of PanCancer Atlas) and Gene Expression Omnibus (GEO; GSE135251) databases were used to predict the potential roles of LGALS3BP and TGF β 1 in patients with liver cancer and metabolic dysfunction-associated steatohepatitis (MASH).

2.2 | Clinical samples from Chonnam National University Hwasun Hospital

Tumoral and peri-tumoral normal tissues were collected from 83 patients with HCC (date of visit: from 2017-01-25 to 2021-07-14) at Chonnam National University Hwasun Hospital (CNUHH, Hwasun, Jeollanam-do, South Korea). Clinicopathological characteristics of patients are described in Supplementary Table S1. The present study was approved by the ethics committee of CNUHH

(Approval number: IRB CNUHH-2021-187). Written informed consent was obtained from all the patients.

2.3 | Cell culture

Mouse primary hepatocytes were isolated via in situ collagenase perfusion and separation using the Percoll (Sigma-Aldrich, Burlington, MA, USA) density-gradient method from the livers of 10-week-old male *LGALS3BP*-KI mice and their controllittermates or *LGALS3BP* fl/wt; Alb-Cre mice and their *LGALS3BP* fl/wt littermates. Isolated mouse primary hepatocytes were cultured in Dulbecco's modified Eagle's medium (Gibco, Burlington, MA, USA) containing 10% fetal bovine serum (FBS) with 5×10^5 cells per well in six-well plates for 40 h before analysis. Mouse HCC (Hepa-1c1c7) and human HCC cells (HepG2, Hep3B and SNU449) were purchased from the American Type Culture Collection (ATCC, Manassas, VA, USA) or Korean cell line bank (KCLB, Seoul, South Korea). All cells in this study were cultured in the recommended medium as alpha minimum essential medium (Gibco) for Hepa-1c1c7, Dulbecco's Modified Eagle's Medium for Hep3B, Eagle's minimum essential medium (Sigma-Aldrich) with 25 mmol/L sodium bicarbonate for HepG2, or RPMI-1640 medium (Sigma-Aldrich) for SNU449 cells, containing 10% fetal bovine serum (Sigma-Aldrich) and 1% penicillin and streptomycin (Invitrogen). To evaluate the gene regulation effects of recombinant proteins, cells were serum-starved for 16 h followed by the treatment with different concentrations of recombinant IFN- α (rIFN- α), recombinant LGALS3BP (rLGALS3BP) or recombinant TGF- β 1 (rTGF- β 1) for subsequent whole-cell extract purification or total RNA isolations.

2.4 | Animals

All animal experiments were performed in specific pathogen-free facilities at Chonnam National University Medical School, according to the guidelines of the Institutional Animal Care Committee (CNU IACUC-H-2021-7). *LGALS3BP*-KO mice were generated using the clustered regularly interspaced short palindromic repeats (CRISPR)-associated protein 9 editing system (Macrogen, Seoul, South Korea) with two single-guide RNAs (sgRNAs, 5'-GCCAGGCAATGGCTCTCCTGTGG-3' and 5'-CTGTGTTCTTGCTGGTTCCAGGG-3') targeting exon 3 of *LGALS3BP* as previously described [31]. Briefly, the sgRNAs and Cas9 recombinant proteins were co-injected into the embryos of C57BL/6N mice (Orient Bio, Seongnam, South Korea), which were then implanted into the oviducts of foster mothers to obtain newborn pups. *LGALS3BP*-KO mice were screened using PCR, the T7E1

assay, and sequencing of tail genomic DNA. The PCR primers used for genotyping are listed in Supplementary Table S2. The T7E1 assay was performed using T7 Endonuclease I (M0302L) according to the manufacturer's instructions (NEB, Ipswich, MA, USA). Heterozygous *LGALS3BP*-KO mice were further bred on C57BL/6J genetic background mice for at least six generations and intercrossed to obtain homozygous *LGALS3BP*-KO mice and its control wild type littermates. The hepatocyte-specific *LGALS3BP*-knockin (KI) mouse was developed using the Cre-/Loxp recombinant enzyme system (MacroGen). Briefly, a silenced C-terminal Myc-tagged *LGALS3BP*-KI cassette under the control of LoxP sites was introduced into the ubiquitously expressed Rosa26 locus of C57BL/6J mouse embryos. Newborn heterozygous *LGALS3BP*-KI pups were screened and bred on a C57BL/6J genetic background for at least four generations. Alb-Cre mice were used to obtain mice with hepatocyte-specific *LGALS3BP* overexpression in *LGALS3BP* fl/wt; Alb-Cre mice. For the carbon tetrachloride (CCl_4)-induced liver fibrosis model [32, 33], 18-week-old male C57BL/6J mice were injected intraperitoneally (IP) with CCl_4 (0.5 $\mu\text{L/g}$, 1:3, v/v in corn oil; #289116, Sigma) or vehicle (dimethyl sulfoxide in corn oil) twice per week for 4 or 6 weeks. Animals were euthanized by cervical dislocation 72 h after the final CCl_4 injection, and whole livers and sera were collected. For the mouse MASH model, 8-week-old male wild type C57BL/6J mice were purchased (Orient Bio, Seongnam, South Korea) and acclimated to a 12 h light/dark cycle at $22 \pm 2^\circ\text{C}$ for 2 weeks. The mice were divided into two groups: the control group was fed a normal chow diet and the MASH group was fed a high-fat methionine-choline-deficient (HFMCD) diet with l-amino acids, 60% calories from fat, 0.1% methionine, and no added choline (A06071302, Research Diets, New Brunswick, NJ, USA) for 5 weeks before being sacrificed. For the diethylnitrosamine (DEN)-high-fat diet (HFD) model of liver carcinogenesis [34], 2-week-old male *LGALS3BP*-KO mice and their littermates were injected with DEN (25 mg/kg body weights, 442687, Merck-Millipore, Burlington, MA, USA). The mice were fed HFD (D12492, Research Diets, New Brunswick, NJ, USA) for 26 weeks until they were sacrificed. The tumors in each liver lobe were counted and measured. Tumors, non-tumor tissues, and serum samples were collected for further analysis.

2.5 | Enzyme-linked immunosorbent assay (ELISA)

The levels of *LGALS3BP* protein were assessed in mouse serum using a mouse Mac-2 binding protein assay kit

(27796, Immuno-Biological Lab, Japan). Conditioned media (CM) derived from Hepa-1c1c7, SNU449, or HepG2 cell cultures under the indicated conditions with r*LGALS3BP* treatment were collected and stored at -20°C . To evaluate the influence of integrin αV or FAK inhibition on the regulation of TGF- β 1 by *LGALS3BP*, cells were pre-incubated with 0.5 ng/mL for Hepa-1c1c7 or 1 ng/mL for human HCC cell lines of GLPG0187 (HY-100506, MedChemExpress, Monmouth Junction, NJ, USA) or 1 $\mu\text{mol/L}$ Defactinib (HY-12289, MedChemExpress) for 1 hour before being exposed to r*LGALS3BP*. The concentration of TGF- β 1 in the conditioned media was assessed using TGF- β 1 DuoSet ELISA kits (DY1679 for mouse or DY240 for human TGF- β 1, R&D Systems) according to the manufacturer's instructions. Briefly, to measure concentrations of total latent TGF- β 1, the CM were activated with acids treatment and stopped for the subsequent quantification. The free active forms of TGF- β 1 in the CM were quantified without acid activation.

2.6 | Western blotting

Whole cell extracts from mouse liver tissues, cultured mouse primary hepatocytes, or Hepa-1c1c7, HepG2, or SNU449 cell lines were prepared in standard radio-immunoprecipitation assay buffer (Invitrogen) and separated by Sodium dodecyl-sulfate polyacrylamide gel electrophoresis (SDS-PAGE) and transferred to polyvinylidene fluoride (PVDF) membranes (Invitrogen). Membranes were probed with primary antibodies and secondary peroxidase-conjugated antibodies (Jackson Immuno-Research, West Grove, PA, USA) and developed using Western BLoT Ultra-Sensitive Horseradish peroxidase Substrate (Takara, Kusatsu, Japan). Signal intensities were detected using an Image Quant LAS 4000 mini (Minato City, Tokyo, Japan). Primary antibodies against phosphorylated Mothers against decapentaplegic homolog 2 (SMAD) family member 2 (p-Smad2, #3108, 1:3,000, Cell signaling technology [CST], Danvers, MA, USA), Smad2 (#5339, 1:3,000, CST), JunB (#3753, 1:3,000, CST), β -actin (#8457, 1:3,000, CST), Myc tag (M192-3, 1:3,000, Medical & Biological Laboratories, Tokyo, Japan), Cyclophilin C-associated protein (CyCAP)/mouse *LGALS3BP* (#28128, 1:1,000, Immuno-Biological Lab, Japan, Fujioka, Japan), TGF- β 1 (ab215715, 1:3,000, Abcam), Integrin subunit alpha V (ITGaV, #60896, 1:3,000, CST), Phosphorylated focal adhesion kinase (FAK) (#3283, 1:3,000, CST), FAK (#3285, 1:3,000, CST) and vascular cell adhesion molecule 1 (VCAM1, ab134047, 1:3,000, Abcam).

2.7 | Hematoxylin and eosin (H&E), Sirius Red, Masson's trichrome (MT), and immunohistochemistry staining

Paraffin-embedded mouse liver tissues were sectioned (4- μ m thick) and subjected to H&E (BBC Biochemical, Mount Vernon, WA, USA), Sirius Red (ab150681, Abcam), MT (ab150686, Abcam), and immunohistochemical staining with alpha-smooth muscle actin (α -SMA) antibodies (ab5694, 1:1,000, Abcam, Waltham, Boston, USA), TGF- β 1 (ab215715, 1:1,000, Abcam), JunB (#3753, 1:3,000, CST), Ki-67 (ab16667, 1:3,000, Abcam) and a secondary antibody (ab6721, 1:1,000, Abcam). To ensure the specificity of staining, negative controls were prepared by incubating the sections with the secondary antibody alone. Additionally, hydrogen peroxidase and BSA were applied to block endogenous peroxidase activity and prevent non-specific binding. Bright-field images of histological sections were captured using a Zeiss Axio Scan Z1 slide scanner (Carl Zeiss, Baden-Württemberg, Germany). The quantification of the intensities of Sirius Red, MT, α -SMA, and TGF- β 1 positively stained areas was carried out using Fiji software (version 2.14.0; National Institutes of Health, Bethesda, MD, USA) by setting and adjusting intensity thresholds based on control samples to ensure consistent detection and measurement of the mean pixel intensity. Positive nuclei for JunB and Ki-67 staining were counted and quantified using Fiji software. The intensity threshold was set to differentiate positive nuclei from the background, and the mean intensity of pixels above this threshold was measured.

2.8 | Quantitative reverse transcription-polymerase chain reaction (qRT-PCR)

Total RNA from human tumoral or peri-tumoral normal tissues of CNUHH patients with HCC, mouse liver tissues, cultured mouse primary hepatocytes, or Hepa-1c1c7, SNU449, Hep3B, and HepG2 cell lines were isolated using a Ribospin II Kit (314-103, GeneAll Biotechnology, Seoul, South Korea) and reverse-transcribed to cDNA using a GoScript reverse transcriptase kit (A5001, Invitrogen, Carlsbad, CA, USA). qRT-PCR was performed using SYBR Green PCR Master Mix (PB20, PCR Biosystems, PA, USA) and the appropriate primers (Supplementary Table S3) with cDNAs using the CFX Connect Real-Time PCR Detection System (Bio-Rad Hercules, CA, USA). The thermocycling conditions were set as follows: 95°C for 3 min, followed by 40 cycles of amplification at 95°C for 10 s, 60°C

for 10 s and 72°C for 30 s. The reaction was completed by determining the dissociation curve of all amplicons.

2.9 | RNA-sequencing (RNA-seq) analysis

Total RNA was extracted from cultured mouse primary hepatocytes from *LGALS3BP*-KO and its control mice or Hepa-1c1c7 cells treated with vehicle or 5 μ g rLGALS3BP (5608-GA; R&D Systems, Minneapolis, MN, USA) using a Ribospin II Kit (Geneall Biotechnology, Seoul, South Korea). Total RNA (1 μ g) was used to prepare an mRNA sequencing library using the MGIEasy RNA Directional Library Prep Kit (MGI Tech, San Jose, CA, USA). The synthesized DNA-nanoball library was quantified using a QuantiFluor DNA System (Promega, Madison, WI, USA). Sequencing was conducted using the MGISEQ-2000 system (MGI Tech) with paired-end 100-base pair reads. Adapter sequences and low-quality bases in the raw reads were trimmed using Skewer (Version 0.2.2, <https://sourceforge.net/projects/skewer>). The remaining high-quality reads were mapped to the reference genome using STAR (2.5). Differentially expressed genes (DEGs) were defined as those showing a >2-fold change between control hepatocytes and *LGALS3BP*-KO primary hepatocytes and a >1.5-fold change between vehicle-treated and rLGALS3BP-treated Hepa-1c1c7 cells. Volcano plots were constructed using the DEGs with Prizm software, and Reactome and Bioplanet biological pathways and transcription factor, protein-protein interaction (PPI) network were predicted using the Enrichr website [35]. RNA-seq data from Hepa-1c1c7 or primary hepatocytes were deposited in the GEO database under accession codes GSE271352 and GSE271355, including all raw and processed data.

2.10 | Short-interfering RNA (siRNA) experiments

siRNA-mediated knockdown experiments were performed with two independent mouse *JUNB*, mouse *LGALS3BP*, or human *LGALS3BP* siRNAs (Bioneer, Daejeon, South Korea; Supplementary Table S4) using Lipofectamine RNAi-MAX (Thermo Fisher Scientific, MA, USA). Following transfection, the cells were incubated for 24 h, serum-starved for 16 h, and treated with 5 μ g/mL of rLGALS3BP and/or 0.5 ng/mL of GLPG0187. The total RNA and whole-cell extracts were prepared for qRT-PCR and western blotting, respectively.

2.11 | Assay for transposase-accessible chromatin with sequencing (ATAC-seq)

ATAC-seq was performed with Hepa-1c1c7 cells treated with vehicle or 5 µg/mL rLGALS3BP using an ATAC-seq Kit (C01080002, Diagenode, NJ, USA). Briefly, the cells were lysed and genomic DNA was transposed simultaneously in a transposition mix. After tagmentation, the transposed DNA fragments were purified and amplified using PCR. The final libraries were purified using AmPure XP Magnetic Beads (Beckman Coulter, Brea, CA, USA), quantified using a Qubit 2.0 Fluorometer (Thermo Fisher Scientific), and sequenced using the NovaSeq platform (Illumina, CA, USA). Potential sequence adapters and low-quality reads were trimmed using the Skewer software. The cleaned quality reads were mapped to the reference genome using bowtie2 (2.3.2). We performed strand cross-correlation analysis to check the suitability of ATAC-seq data for further analysis. MACS2 (2.1) with 'default' or 'broad' parameters was used to identify the significantly enriched regions. Motif enrichment in peaks was performed using findMotifGenome.pl in Homer (4.9) [36]. ATAC-seq data were deposited in the GEO database under the accession code GSE271354, including all raw and processed data.

2.12 | Activator protein-1 (AP-1) reporter assays

Hepa-1c1c7, SNU449, or HepG2 cells were seeded to transiently transfect AP-1 reporter (631906, Clontech, CA, USA) in 96-well plates using Lipofectamine 3000 (Thermo Fisher Scientific). Culture media was changed into serum free medium 20 h following transfection and then treated with increased amounts of rLGALS3BP. Cells were subsequently washed with PBS, lysed for Dual luciferase assay (E1910, Promega, MI, USA), and reporter activities were measured by luminometer (SpectraMax, i3X, Molecular devices, CA, USA).

2.13 | Chromatin immunoprecipitation (ChIP) analysis

ChIP assays to validate JunB binding at *TGFBI* promoter were performed using Hepa-1c1c7 cell lysates and an EZ-ChIP Kit (17-371, Merck-Millipore, Burlington, MA, USA) with α-JunB (#3753, CST) or normal rabbit IgG (#2729, CST). Briefly, formaldehyde-cross-linked cells were lysed and sonicated to prepare genomic DNA fragments (200–500 bp). For each assay, 4 µg of antibody was used to immunoprecipitate 40 µg of input chromatin. Immune

complexes were recovered using 30 µL of resuspended protein A/G agarose. After washing, the DNA was de-crosslinked and eluted, as described in the manufacturer's instructions. qPCR was performed in a 7500 Fast Thermal Cycler (Life Technologies, Carlsbad, CA, USA), using the ChIP primers listed in Supplementary Table S3.

2.14 | Liquid chromatography-tandem mass spectrometry (LC-MS/MS)

Whole-cell extracts of primary hepatocytes isolated from *LGALS3BP*-KI mice were prepared to identify the PPI network using Myc-tagged *LGALS3BP*. One-milliliter pellets of primary hepatocytes were sonicated in 2.5 mL lysis buffer (25 mmol/L Tris-Cl pH 7.4, 150 mmol/L KCl, 1 mmol/L Ethylenediamine tetraacetic acid, 0.5% NP40, protease inhibitors) and immunoprecipitated. Following incubation with agarose beads or anti-Myc-conjugated agarose beads at 4°C for 2 h, the pellets were washed three times with lysis buffer and twice with phosphate-buffered saline. The precipitated proteins were digested and reconstituted with 0.1% formic acid in LC-MS grade water and analyzed using a Dionex UltiMate 3000 nano LC system connected to an Orbitrap Fusion Lumos MS equipped with an EASY-Spray ion source (Thermo Fisher Scientific).

2.15 | Co-immunoprecipitation assay

Hepa-1c1c7 and SNU449 cells were transfected with a vector encoding Myc-tagged *LGALS3BP* or the parental vector, cultured for 40 h, and incubated in serum-free medium for 16 h. Ten milliliters of conditioned medium from each plate was incubated with anti-Myc-conjugated agarose beads, washed, and then incubated with Hepa-1c1c7 whole-cell extracts prepared with Pierce IP lysis buffer (#87787, Thermo Fisher Scientific). Following incubation at 4°C for 2 h, the beads were washed twice with Pierce IP lysis buffer (25 mmol/L Tris-Cl, pH 7.4, 150 mmol/L KCl, 1 mmol/L Ethylenediaminetetraacetic acid, 0.5% NP40, and protease inhibitors) and once with lysis buffer containing 300 mmol/L NaCl. Bead-bound proteins were resolved by SDS-PAGE followed by western blotting with antibodies against ITGαV (#60896, 1:3,000), ITGα5 (#4705, 1:3,000), and ITGβ1 (#34971, 1:3,000) from CST or an anti-Myc tag antibody (M192-3) from MBL with indicated dilutions.

2.16 | Immunofluorescence staining

Hepa-1c1c7, HepG2, and SNU449 cells were subjected to immunofluorescence (IF) staining. Briefly, cells were fixed

with 4% paraformaldehyde for 10 min, followed by permeabilization with 0.1% Triton X-100 for 15 min. After rinsing the samples with 1x PBS, a solution of 1% bovine serum albumin and 0.5% Tween-20 was applied to block non-specific antibody-binding sites. Anti-p-FAK (PA5-85602, Invitrogen), Phalloidin-conjugated Alexa Fluor 647 antibody (A22287, Invitrogen), and 4',6-diamidino-2-phenylindole (DAPI) were used to label the phosphorylated FAK, filamentous actin (F-actin), and nuclei, respectively. To detect the ITG α V accumulation by LGALS3BP overexpression, HepG2 cells were seeded on poly-L-lysine (P4707, Sigma-Aldrich) coated eight well chambers (154534, Thermo Fisher Scientific). After 24 h, when cells achieved 70%–80% confluence, transfections were carried out with Lipofectamine 3000 (Thermo Fisher Scientific) and pcDNA6/myc-LGALS3BP (0.5ug/wells). Cells were fixed with 4% paraformaldehyde, and permeabilized with 0.1% Triton X-100. Myc-tagged LGALS3BP was detected using a mouse Myc-tag antibody (M192-3, MBL) followed by Alexa Fluor 488-conjugated secondary antibody (A32723, Invitrogen). ITG α V (ab179475, Abcam) was detected using rabbit anti-ITG α V antibody followed by Alexa Fluor 647-conjugated secondary antibody (A32733, Invitrogen). For Proximity Ligation Assay (PLA), HepG2 cells were transiently transfected with myc-LGALS3BP expressing vectors on coated eight well chambers (154534, Thermo Fisher Scientific). After 24 h, cells were permeabilized and blocked using a PLA kit (DUO92101, Sigma-Aldrich, St. Louis, MO) according to the manufacturer's instructions. Primary antibodies were incubated with cells for 2 h at 37°C and then washed and incubated with PLA probes. A mounting medium with DAPI (Sigma-Aldrich, St. Louis, MO) was added and cells were visualized under fluorescence with Texas Red filter (excitation 594 nm, emission 624 nm) with a Zeiss LSM 780 laser-scanning confocal microscope. Confocal images were acquired using an Olympus FLUOVIEW FV1000 confocal microscope and quantified using Image J Fiji software (version 2.14.0) and Zen blue 3.1 software (Zeiss, Oberkochen, Germany).

2.17 | Triglyceride quantification

Triglyceride levels were measured in 30 mg homogenized liver tissue or mouse plasma samples using a triglyceride assay kit (ab65336, Abcam) according to the manufacturer's instructions.

2.18 | Oil Red O staining

For frozen sections, the liver tissues were fixed with 4% paraformaldehyde overnight and then infiltrated

with 30% sucrose. The tissues were embedded in OCT compound (Tissue-Tek, Sakura Finetek USA, Torrance, CA) and stored at -80°C until analysis. Frozen tissues were sectioned at 6 μm using a cryostat (CM1860, Leica Biosystems, IL, USA). The sections were then dried, fixed in 10% formalin, and washed with 60% isopropanol. The slides were stained with Oil Red O (O0625, Sigma-Aldrich) working solution for 15 min. The slides were counterstained with hematoxylin and washed with distilled water. Positively stained areas were quantified using Fiji software (version 2.14.0; National Institutes of Health, Bethesda, MD, USA).

2.19 | Statistical analysis

All statistical analyses were performed using GraphPad Prism10 (Graph Pad, San Diego, CA, USA) and values are expressed as the mean \pm standard deviation from three independent experiments, unless otherwise indicated. Student's *t*-test was used to determine the statistical significance between two groups, and two-way analysis of variance (ANOVA) for comparing more than two groups. $P < 0.05$ was considered significant.

3 | RESULTS

3.1 | Correlation of *TGFB1* expression with *LGALS3BP* expression in HCC patients

To investigate the role of LGALS3BP in hepatic carcinogenesis, gene sets positively correlated with *LGALS3BP* expression in TCGA HCC dataset were analyzed using Reactome pathway analysis. As the regulatory role of LGALS3BP in innate immunity and cell-to-cell interactions has been studied, the immune system, signal transduction, and ECM organization genes were found to be significantly co-regulated with *LGALS3BP* expression (Figure 1A and Supplementary Table S5). As matrix metalloproteinase 2 (*MMP2*), *MMP9*, collagen type I alpha 2 (*COL1A2*), and *TGFB1* were common to the pathways (Figure 1B), and MMP and collagen genes are regulated by TGF- β 1 signaling [37–39], we hypothesized that *LGALS3BP* expression was closely associated with *TGFB1* expression.

We examined the correlation between *LGALS3BP* and TGF- β family members *TGFB1*, *TGFB2* and *TGFB3* in primary liver cancer tissues from 83 patients who underwent surgery for HCC. As *LGALS3BP* expression exhibited strong positive correlations with *TGFB1* in TCGA HCC data, *LGALS3BP* expression in HCC tumors at CNUHH also exhibited strong positive correlation with *TGFB1*. *LGALS3BP* had relatively weaker positive correlations

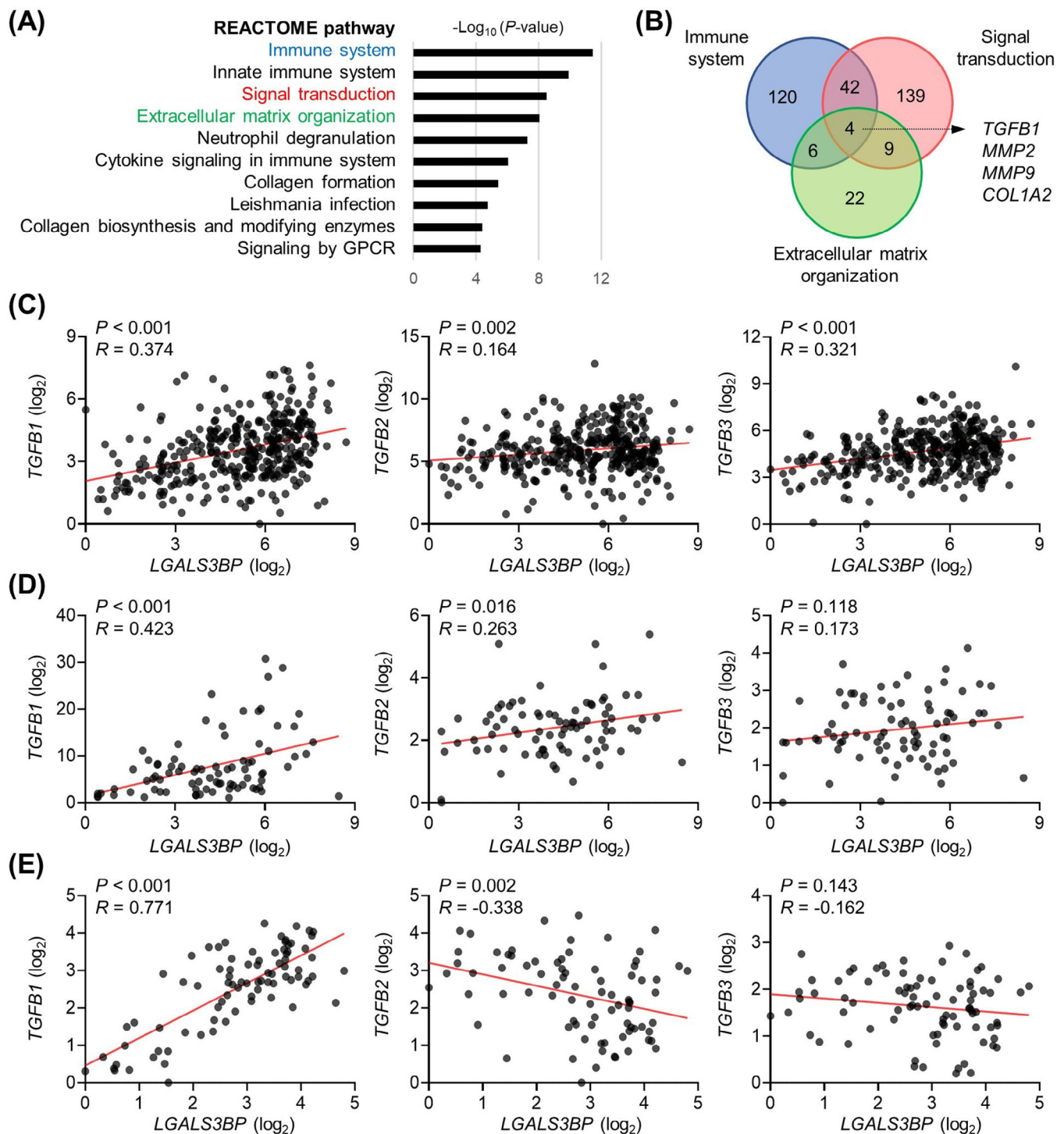


FIGURE 1 Correlation of *TGFBI* expression with *LGALS3BP* expression in HCC patients. (A) Reactome pathway analysis of genes that showed a positive correlation with *LGALS3BP* expression in TCGA HCC data ($n = 366$). (B) Venn diagram showing common genes between the gene sets. (C) The correlation between *LGALS3BP* and *TGFBI*, *TGFBI*, or *TGFBI* levels in HCC from TCGA dataset ($n = 366$). (D) The correlation between *LGALS3BP* and TGFBI family members in tumoral tissues of HCC patients at CNUHH ($n = 83$). (E) The correlation between *LGALS3BP* and TGFBI family members in peri-tumoral normal tissues of HCC patients at CNUHH ($n = 83$). The Pearson's correlation coefficient (R) and two-tailed P values are indicated in each graph. Abbreviations: CNUHH, chonnam national university hwasun hospital; *COL1A2*, collagen type I alpha 2; HCC, hepatocellular carcinoma; *LGALS3BP*, lectin galactoside-binding soluble 3 binding protein; *MMP2*, matrix metalloproteinase 2; *MMP9*, matrix metalloproteinase 9; TCGA, the cancer genome atlas; *TGFBI*, transforming growth factor beta 1.

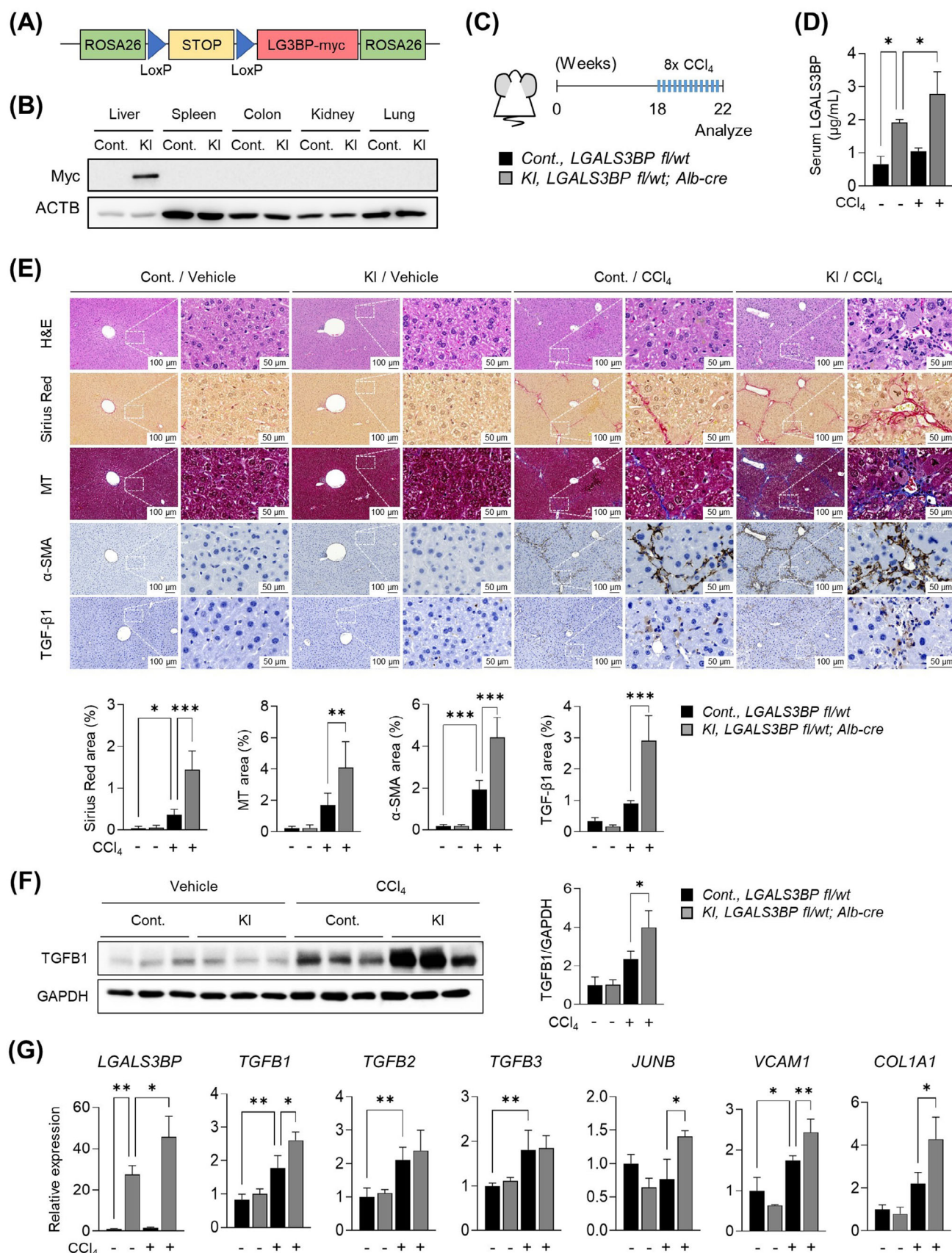


FIGURE 2 Effect of hepatic *LGALS3BP* overexpression on *TGFβ1* upregulation and exacerbation of CCl₄-induced hepatic fibrosis. (A) Schematic illustration of *LGALS3BP*-KI construct. The myc-epitope-tagged *LGALS3BP* was ectopically expressed by the removal of long poly-A sequences (STOP) with Cre recombinase. (B) Western blotting to detect ectopic *LGALS3BP* expression in whole-cell lysates from

with *TGFB2* and *TGFB3* (Figure 1C-E), suggesting its specialized role in *TGFB1* regulation.

3.2 | IFN- α induced *LGALS3BP* for *TGFB1* expression

Treatment with IFN- α , a critical regulator of *LGALS3BP* expression, increased *TGFB1* mRNA levels in rat pre-neoplastic liver cells, and IFN- α and TGF- β 1 cooperated to induce liver fibrosis [40, 41]. To determine whether *LGALS3BP* regulates *TGFB1* in this context, the effects of IFN- α on murine hepatic carcinoma Hepa-1c1c7 cells were tested. The rIFN- α treatment induced the expression of *LGALS3BP* and interferon regulatory factor 7 (*IRF7*) significantly, along with that of *TGFB1* (Supplementary Figure S1A), and the knockdown of *LGALS3BP* using two separate siRNA constructs blocked IFN- α -dependent *TGFB1* expression significantly (Supplementary Figure S1B). Notably, the mRNA expression of IFN- α -induced genes (*IRF7* and *MX2*) and TGF- β 1 target genes (*VCAM1* and *COL1A1*) were positively associated with *LGALS3BP* expression in the tumoral and peri-tumoral normal tissues of HCC patients (Supplementary Figure S2).

3.3 | Effect of hepatic *LGALS3BP* overexpression on *TGFB1* upregulation and exacerbation of CCl₄-induced hepatic fibrosis

To investigate the role of *LGALS3BP* in *TGFB1* regulation in vivo, we generated a conditional knockin (KI) mouse model wherein hepatocytes specifically overexpressed *LGALS3BP* (Figure 2A). *LGALS3BP* was exclusively expressed in the liver tissues of transgenic mice when mated with Alb-Cre mice (Figure 2B). Primary hepatocytes isolated from *LGALS3BP*-KI mice exhibited significantly elevated *TGFB1* levels along with *LGALS3BP* overexpression (Supplementary Figure S3A). Known TGF- β 1-target

genes, such as *VCAM1*, *LIF*, *PDGFB*, and *COL1A1*, were induced in *LGALS3BP*-KI primary hepatocytes (Supplementary Figure S3A). Culture medium and whole-cell extracts from primary *LGALS3BP*-KI hepatocytes showed the induced *LGALS3BP* protein secretion and elevated pro-TGF- β 1 levels (Supplementary Figure S3B).

We used a CCl₄-induced model of hepatic fibrosis to demonstrate the role of *LGALS3BP* in hepatic fibrosis in vivo (Figure 2C) as dysregulated TGF- β 1 signaling regulates the progression of the disease [26]. Hepatocyte-specific overexpression in *LGALS3BP*-KI mice resulted in higher circulating serum *LGALS3BP* levels than in their control littermates (Figure 2D). The liver tissues of CCl₄-treated mice exhibited a distorted structure, with micronodules noted throughout the liver parenchyma along with fibrosis symptoms, as determined by measuring the accumulation of collagen fibers and α -SMA. The *LGALS3BP*-KI mice displayed a more pronounced fibrosis profile in their livers than in those of WT mice (Figure 2E). We found that the expression of TGF- β 1 was significantly higher in the livers of *LGALS3BP*-KI mice than in those of control mice following intraperitoneal CCl₄ injection (Figure 2F) along with the expression of TGF- β 1 target genes (Figure 2G).

3.4 | Induction of *TGFB1* and its target gene expression by r*LGALS3BP* treatment

The fibrosis-promoting role of *LGALS3BP* prompted us to investigate whether secreted *LGALS3BP* directly regulates *TGFB1* expression. Surprisingly, treatment with r*LGALS3BP* alone was sufficient to stimulate *TGFB1* expression and its canonical downstream signaling mediator, Smad2 phosphorylation, in Hepa-1c1c7 cells (Figure 3A-B). Compared with 5 μ g/mL, 20 μ g/mL of r*LGALS3BP* did not enhance the *TGFB1* induction probably due to the induced SMAD6, a negative regulator for SMAD signaling at this condition (Supplementary Figure S4).

indicated tissues. (C) Experimental outline of the mouse model of hepatic fibrosis. *LGALS3BP* fl/wt or *LGALS3BP* fl/wt; Alb-Cre mice were intraperitoneally injected with CCl₄ twice per week for 4 weeks. All the mice were euthanized at 22 weeks of age. (D) ELISA assays to measure serum *LGALS3BP* levels at the time of the sacrifice. Data represented as mean \pm SD, $n = 3$ (vehicle injected group) or $n = 5$ (CCl₄ injected group). * $P < 0.05$, ** $P < 0.01$, and *** $P < 0.001$ (Two-way ANOVA). (E) Representative images of H&E, Sirius Red, MT staining, immunohistochemical staining of α -SMA or TGF- β 1 in the liver tissues of the indicated mice. Quantification of the positively stained area were shown below. The stained areas were shown as percentages of the total area of each liver sections. Data represented as mean \pm SD, $n = 4-9$. * $P < 0.05$, ** $P < 0.01$, and *** $P < 0.001$ (Two-way ANOVA). (F) Representative TGF- β 1 western blotting of each group using whole-cell extracts from liver tissues. Quantification of the band intensities were shown on the left. (G) qRT-PCR analysis of the indicated genes. Data represented as mean \pm SD, $n = 3$ (vehicle injected groups) or $n = 5$ (CCl₄ injected groups). * $P < 0.05$, ** $P < 0.01$, and *** $P < 0.001$ (Two-way ANOVA). Abbreviations: Alb-cre, albumin promoter controlled cre recombinase; *COL1A1*, collagen type I alpha 1; Cont., control; fl/wt, floxed and wild type; H&E, hematoxylin and eosin stain; KI, knockin; LG3BP-myc, myc epitope tagged lectin galactoside-binding soluble 3 binding protein; MT, Masson's trichrome stain; *VCAM1*, Vascular cell adhesion protein 1; α -SMA, alpha-smooth muscle actin.

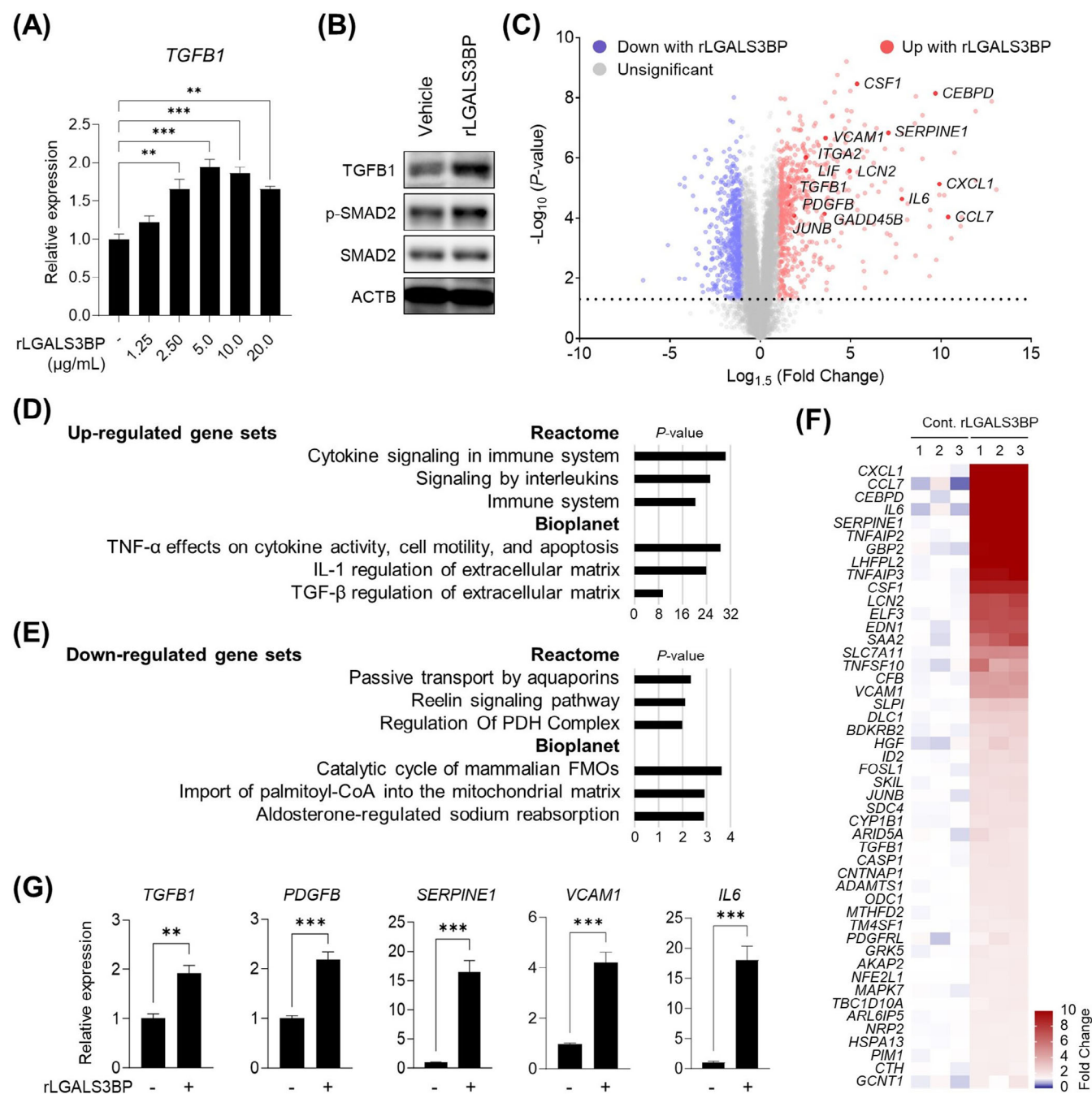
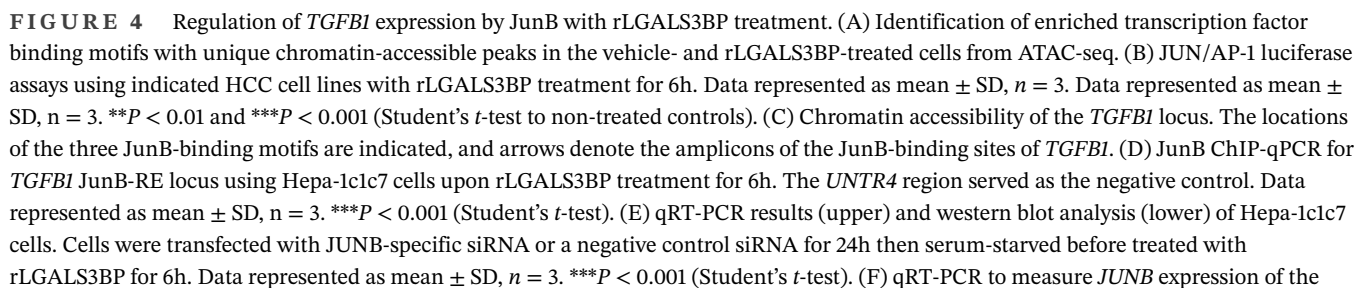


FIGURE 3 Induction of TGFβ1 and its target gene expression by recombinant LGALS3BP treatment. (A) qRT-PCR of *TGFβ1* expression in Hepa-1c1c7 cells treated with indicated concentration of rLGALS3BP for 6 h. (B) Representative western blotting of whole-cell extracts from rLGALS3BP treated Hepa-1c1c7 cells. (C) Volcano plots showing differentially expressed genes upon rLGALS3BP treatment (compared to the vehicle-treated group; $n = 3$). (D) Pathway analyses of the upregulated gene sets upon rLGALS3BP treatment. (E) Pathway analyses of the downregulated gene sets upon rLGALS3BP treatment. (F) Heatmap of genes involved in TGF-β regulation of extracellular matrix of the Bioplanet pathway indicated in (D). (G) qRT-PCR validation of the RNA-seq results. Data represented as mean \pm SD, $n = 3$. ** $P < 0.01$ and *** $P < 0.001$ (Student's t -test). Abbreviations: DEG, differentially expressed genes; *IL6*, interleukin-6; *PDGFB*, platelet derived growth factor subunit B; p-SMAD2, phosphorylated SMAD2; rLGALS3BP, recombinant LGALS3BP; *SERPINE1*, serine proteinase inhibitor E1; SMAD2, mothers against decapentaplegic homolog 2; TGFβ1, transforming growth factor beta 1; *VCAM1*, vascular cell adhesion protein 1.



We examined the impact of gene expression in Hepa-1c1c7 cells using RNA-seq following exposure to rLGALS3BP (Figure 3C). Pathway analysis of the upregulated gene sets revealed the activation of multiple signaling pathways by inflammatory cytokines, including TNF- α , interleukins, and TGF- β 1 (Figure 3D and Supplementary Table S6). Genes downregulated by rLGALS3BP treatment indicated that the metabolism of free fatty acids, such as the regulation of the pyruvate dehydrogenase complex and import of palmitoyl-coenzyme A into the mitochondrial matrix, was decreased (Figure 3E and Supplementary Table S7). The genes associated with the regulation of TGF- β on ECM was increased significantly, including known targets of TGF- β 1, such as *SERPINE1*, *VCAM1*, and *IL6* (Figure 3F), along with the upregulation of another TGF- β 1 target gene, *PDGFB* (Figure 3G).

3.5 | Regulation of TGFB1 expression by JunB with rLGALS3BP treatment

To define the underlying mechanisms via which *TGFB1* expression is controlled directly, the alternation of transcription factor binding upon rLGALS3BP treatment was analyzed using ATAC-seq. Differentially accessible regions were curated for motif analysis, and one distinct transcription factor that exhibited changes in accessibility was JunB (Figure 4A), which has been studied for its role in regulating *TGFB1* expression [42–45]. Transactivation of AP-1 luciferase reporter activated by transcription factors including JunB-binding sites was induced by rLGALS3BP treatment in various HCC cell lines (Figure 4B). Notably, the chromatin-accessible region around the *TGFB1* locus contained three JunB-response sequences (Figure 4C). The rLGALS3BP-inducible JunB binding to ATAC peak regions was validated independently by JunB ChIP-qPCR (Figure 4D). *JUNB* knockdown using siRNA abolished the rLGALS3BP-promoted TGF- β 1 expression completely (Figure 4E). Primary hepatocytes isolated from *LGALS3BP*-KI cells showed higher *JUNB* expression than those from the controls (Figure 4F). Using TCGA HCC data and CNUHH HCC patient tissues, a positive correlation between *JUNB* and *LGALS3BP* expression was identified (Figure 4G–I).

3.6 | Interaction of LGALS3BP with ITG α V and promotion of ITG α V accumulation on the cell membrane to release TGF- β 1

We observed an unexpected trend in *TGFB1* mRNA expression and the amount of secreted total TGF- β 1 in the culture medium upon rLGALS3BP treatment. The released active form of TGF- β 1 peaked at 3 h, and even secreted total TGF- β 1 levels were not altered, whereas *TGFB1* mRNA expression increased gradually over time (Figure 5A, Supplementary Figure S4).

LC-MS/MS proteomics was conducted to gain insight into the mechanism of TGF- β 1 release (Figure 5B). Interestingly, one network (cluster 4) interacting with LGALS3BP contained ITG α V among the 30 LGALS3BP-interacting protein clusters, and the enhanced network revealed the physical interactions between ITG α V and TGF- β 1 (Figure 5C and Supplementary Figure S5A–B). The physical interaction was validated by an immunoprecipitation assay using the isolated LGALS3BP from the culture medium and ITG α V in SNU449 and Hepa-1c1c7 cell extracts (Figure 5D and Supplementary Figure S5C).

To determine the role of ITG α V in LGALS3BP-mediated TGF- β 1 activation, we utilized GLPG0187, an ITG α V inhibitor that has been studied as a drug that suppresses the growth of various metastatic tumors [46] and more recently SARS-CoV-2 delta infections [46, 47]. GLPG0187 effectively inhibited the release of active TGF- β 1 triggered by LGALS3BP in HCC cells, (Figure 5E). Physical interaction between transiently transfected LGALS3BP and ITG α V was observed (Figure 5F), and ectopic expression of LGALS3BP led to the ITG α V accumulation (Figure 5G). Upon rLGALS3BP treatment, ITG α V on the cell membrane was accumulated, and the number of filamentous actins (F-actin) in the cytosolic region was increased significantly (Figure 5H–I). The inhibition of ITG α V caused the reduction of the increased JunB binding to the promoter region of *TGFB1* by rLGALS3BP treatment (Figure 5J). FAK is a primary intracellular downstream mediator that delivers signals from ITG α V [48, 49]. Notably, when Hepa-1c1c7 cells were treated with Defactinib, a chemical inhibitor of FAK, free TGF- β 1 levels was significantly suppressed (Figure 5K).

control and *LGALS3BP*-KI primary hepatocytes. Data represented as mean \pm SD, $n = 3$. *** $P < 0.001$ (Student's t -test). (G) The correlation between *LGALS3BP* and *JUNB* in HCC from TCGA dataset ($n = 366$). (H) The correlation between *LGALS3BP* and *JUNB* in tumoral tissues of HCC patients at CNUHH ($n = 83$). (I) The correlation between *LGALS3BP* and *JUNB* in peri-tumoral normal tissues of HCC patients at CNUHH ($n = 83$). * $P < 0.05$, ** $P < 0.01$, and *** $P < 0.001$ (Two-way ANOVA). Abbreviations: ATAC-seq, the assay for transposase-accessible chromatin with sequencing; ATF4, activating transcription factor 4; Cont, control; FOSL2, FOS like 2; FOXA1, forkhead box protein A1; FOXO3, forkhead box protein O3; JUNB-RE, JunB response elements; KI, *LGALS3BP* knockin; rLGALS3BP, recombinant LGALS3BP; TEAD4, TEA domain transcription factor 4; *UNTR6*, untranscribed region 6.

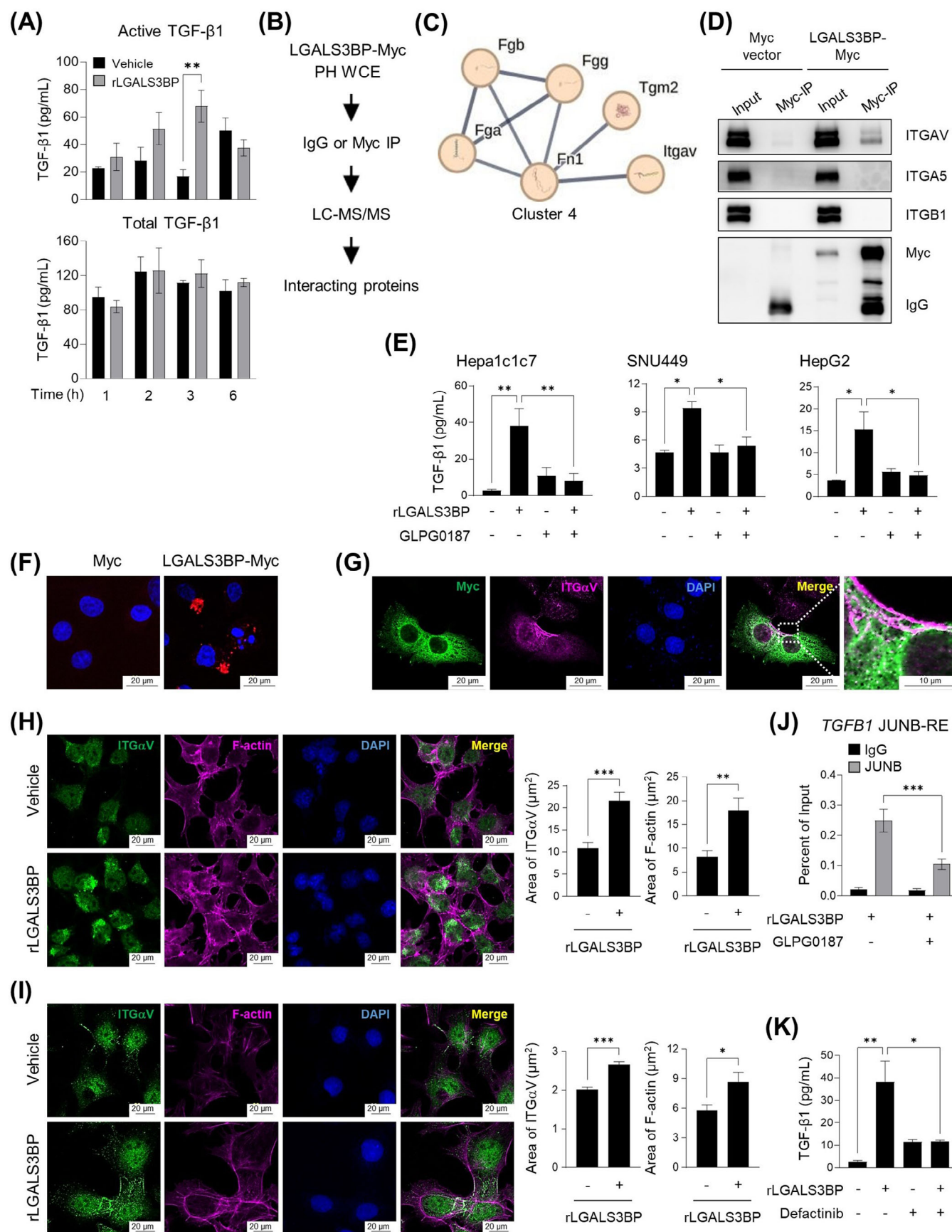


FIGURE 5 Interaction of LGALS3BP with ITG α V and promotion of ITG α V accumulation on the cell membrane to release TGF- β 1. (A) Measurement of active TGF- β 1 and total TGF- β 1 in the culture medium of Hepa-1c1c7 cells upon rLGALS3BP treatment. (B) Experimental

3.7 | JunB-TGF- β 1 feedback loop initiation by LGALS3BP via the activation of ITG α V-mediated rearrangement of F-actin cytoskeleton

The release of active TGF- β 1 from its latent complex requires the application of tensile force, which is generated by the formation of a stiff cytoskeleton modulated by ITG α V-FAK signaling [28-30, 50]. Interestingly, rLGALS3BP treatment led to the increased FAK phosphorylation and the subsequent rearrangement of F-actin cytoskeleton in Hepa-1c1c7 cells (Figure 6A). GLPG0187 was found to efficiently inhibit the activation of p-FAK and F-actin stretching (Figure 6A). Inhibition of ITG α V resulted in decreased *TGFBI* and *JUNB* mRNA expression (Figure 6B). When the cells were treated with rLGALS3BP, expression levels of ITG α V, JunB, and cytosolic pro-TGF- β 1 were significantly induced; the elevated protein levels along with increased phosphorylated FAK were blocked by ITG α V inhibition (Figure 6C). The rearrangement of the cytoskeleton and subsequent gene regulation dependent on ITG α V were also observed in human HCC SNU449 cells upon treatment with rLGALS3BP (Figure 6D-F). Collectively, LGALS3BP triggered active TGF- β 1 release from its latent complex through ITG α V-FAK-mediated stiff F-actin cytoskeleton which is critical for the tensile force generation. rTGF- β 1 treatment promoted the expression of *JUNB* and *TGFBI* (Supplementary Figure S6A), suggesting the positive feedback loop by released TGF- β 1. Since TGF- β 1 transcriptionally promoted *LGALS3BP* expression in rat thyroid FRTL-5 cells [51], we also tested whether rTGF- β 1 treatment increased *LGALS3BP* expression.

Although rLGALS3BP or rTGF- β 1 treatment promoted *TGFBI* expression in Hepa-1c1c7 cells, *LGALS3BP* levels were not changed at these conditions (Supplementary Figure S6B).

3.8 | Downregulation of TGF- β 1 signaling and CCL₄-induced fibrosis by *LGALS3BP* depletion

The observation that the JunB-TGF- β 1 axis was directly regulated by secreted LGALS3BP prompted us to examine the effect of *LGALS3BP* depletion on the regulation of TGF- β 1 signaling in the livers using *LGALS3BP* KO mice (Supplementary Figure S7). As an initial step, we analyzed the expression of altered genes in the isolated primary hepatocytes. DEG analyses between control and *LGALS3BP*-KO primary hepatocytes from RNA-seq analysis revealed significant downregulation of TGF- β 1 and its target genes (Figure 7A). Upregulated genes were associated with multiple metabolic processes, including phenylalanine and tyrosine amino acid metabolism (Figure 7B and Supplementary Table S8). Notably, Reactome gene sets with downregulated genes showed decreased non-ITG membrane and ECM interactions and organization genes (Figure 7C and Supplementary Table S9). Moreover, the upregulated gene sets of Bioplanet pathways in rLGALS3BP-treated cells (Figure 3D) was reversed by the depletion of *LGALS3BP* (Figure 7C). TGF- β signaling mediators, Smad2/3, and its active transcriptional partner Smad4 were predicted to be factors associated with decreased gene sets (Supplementary Figure S8A), and TGF- β 1 target genes, *VCAM1*, *PDGFB*,

outline: whole cell extracts of *LGALS3BP*-KI primary hepatocytes were immunoprecipitated with normal IgG or α -myc. Immunoprecipitants were analyzed by LC-MS/MS. (C) Protein-protein interactions in the cluster 4 among the LGALS3BP-binding protein networks. (D) Co-immunoprecipitation assays to detect the interaction between secreted LGALS3BP and ITG proteins using anti-myc antibody with whole cell extracts of empty vector or myc-LGALS3BP transfected SNU449 cells. (E) ELISA for the detection of active TGF- β 1 in Hepa-1c1c7, SNU447, and HepG2 cells in the culture medium upon rLGALS3BP \pm GLPG0187 treatment. Data represented as mean \pm SD, $n = 3$. * $P < 0.05$ and ** $P < 0.05$ (Two-way ANOVA). (F) Representative images of PLA results using HepG2 cells. Empty vector or myc-epitope tagged LGALS3BP was transiently transfected into HepG2 cells to detect its interaction with ITG α V. Red dots indicate the protein-protein interactions. Blue dots denote DAPI nuclei staining. (G) Immunofluorescence staining of transfected myc-LGALS3BP (Green) and ITG α V (Pink). (H) Immuno-fluorescence staining of ITG α V and F-actin in Hepa-1c1c7 cells upon rLGALS3BP treatment for 1h. Quantification of total stained area of ITG α V and F-actin were shown on the left with five scanned images per slides of three independent experiments. Data represented as mean \pm SD, ** $P < 0.01$ and *** $P < 0.001$ (Student's *t*-test). (I) Immunofluorescence staining of ITG α V and F-actin in HepG2 cells upon rLGALS3BP treatment for 1h. Quantification of total stained area of ITG α V and F-actin were shown on the left with five scanned images per slides of three independent experiments. Data represented as mean \pm SD, * $P < 0.05$ and *** $P < 0.001$ (Student's *t*-test). (J) JunB ChIP-qPCR analysis of *TGFBI* JUNB-RE locus using Hepa-1c1c7 cells upon rLGALS3BP \pm GLPG0187 treatment. Data represented as mean \pm SD, $n = 3$. *** $P < 0.001$ (Student's *t*-test). (K) Measurement of active TGF- β 1 in the culture medium of Hepa-1c1c7 cells upon rLGALS3BP \pm Defactinib treatment. Data represented as mean \pm SD, $n = 3$. * $P < 0.05$, ** $P < 0.01$, and *** $P < 0.001$ (Student's *t*-test). Abbreviations: DAPI, 4',6-diamidino-2-phenylindole; F-actin, filamentous actin; IP, immunoprecipitation; ITG α V, integrin subunit alpha V; JUNB-RE, JunB response elements; LC-MS/MS, Liquid Chromatography with tandem mass spectrometry; PH, primary hepatocytes; PLA, Proximity Ligation Assay; rLGALS3BP, recombinant LGALS3BP; *TGFBI*, transforming growth factor beta 1; WCE, whole cell extract.

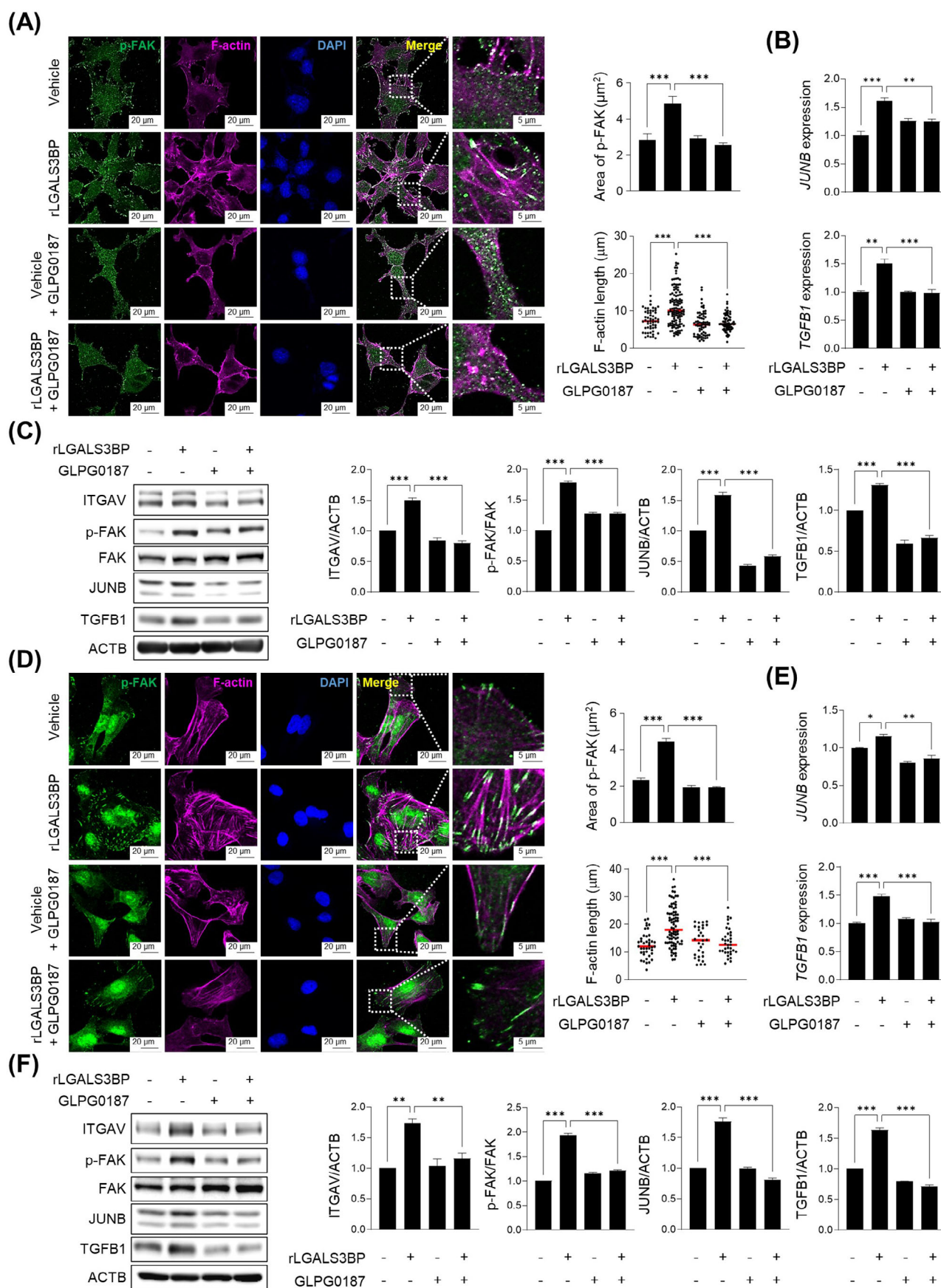


FIGURE 6 JunB-TGF- β 1 feedback loop initiation by LGALS3BP via the activation of ITG α V-mediated rearrangement of F-actin cytoskeleton. (A) Immunofluorescence staining of phosphorylated FAK and F-actin in Hepa-1c1c7 cells upon rLGALS3BP \pm GLPG0187

LIF, and *COL1A1*, were downregulated along with *TGFBI* (Supplementary Figure S8B).

We further examined a CCl₄-induced fibrosis mouse model to demonstrate the role of *LGALS3BP* depletion in vivo (Figure 7D). As expected, induced expression levels of *TGFBI* by hepatic fibrosis were reduced by depleting *LGALS3BP* along with *JUNB* and *COL1A1* significantly (Figure 7E). The livers of *LGALS3BP*-KO mice demonstrated reduced fibrosis compared to those of WT mice, as evidenced by decreased collagen fiber deposition and α -SMA expression (Figure 7F). TGF- β 1, ITG α V, p-FAK, and JunB levels were significantly reduced in *LGALS3BP*-KO mouse livers, (Figure 7G and supplementary Figure S9) as opposed to the stimulation seen in *LGALS3BP*-KI mouse livers (Supplementary Figure S3C).

3.9 | Reduction of the steatohepatitis-induced hepatocarcinogenesis by *LGALS3BP* depletion

We found that MASH severity in human patients was associated with increased *LGALS3BP* along with *TGFBI* and *COL1A1* expression, and *LGALS3BP* and *TGFBI* levels were positively correlated in the patients [52] (GSE135251, Supplementary Figure S10A-C). In fact, *LGALS3BP* expression was elevated significantly along with *TGFBI* in the livers of mice fed a HFMCD diet (Supplementary Figure S10D-E), which is a mouse model for studying MASH [53, 54].

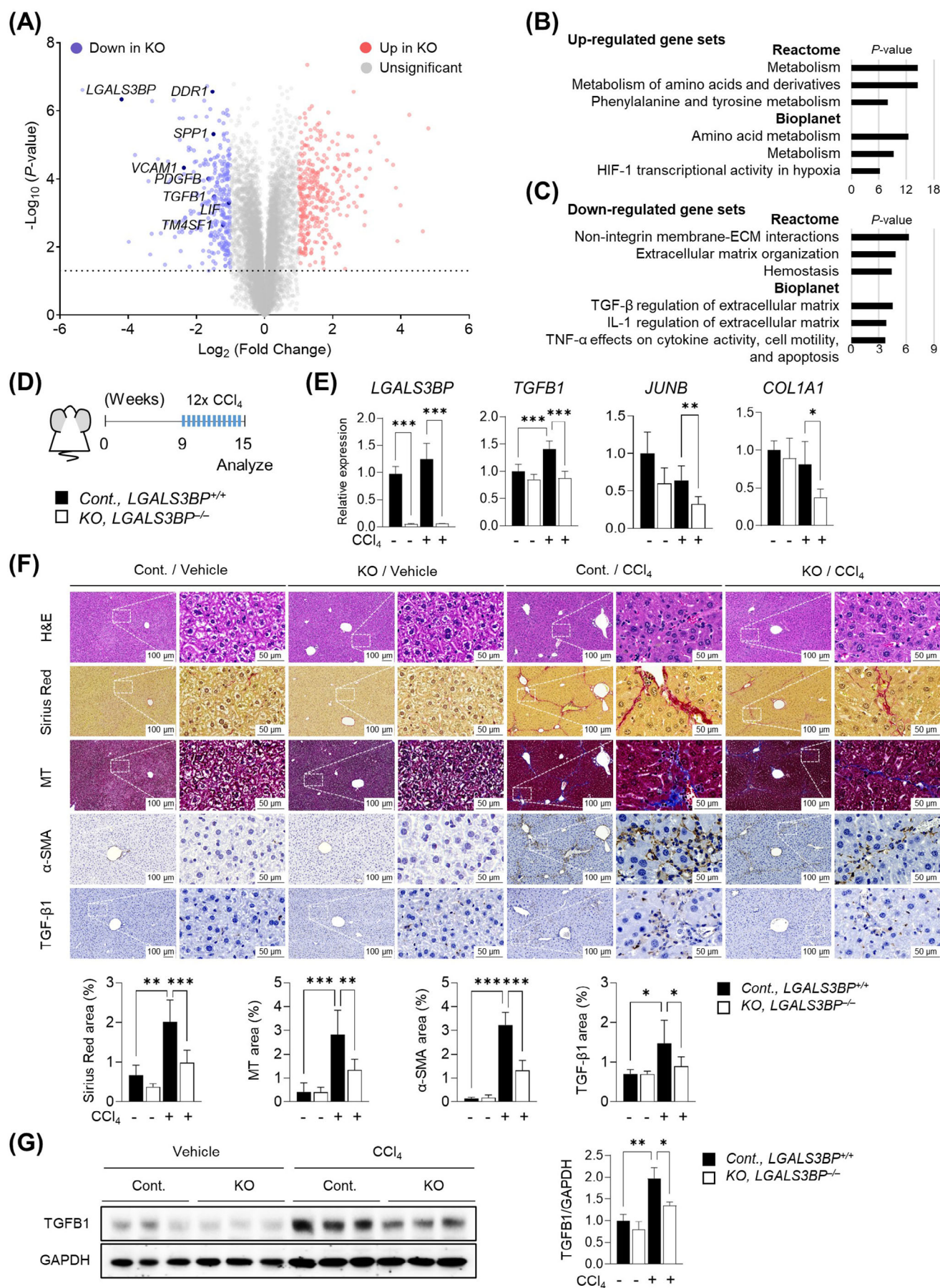
As uncontrolled chronic inflammation-induced hepatic fibrosis is closely associated with the development of hepatic carcinogenesis [32], we investigated whether *LGALS3BP* depletion ameliorates DEN- and HFD-induced hepatic carcinogenesis via regulating TGF- β 1 signaling (Figure 8A). The livers of *LGALS3BP*-KO mice showed a noticeable decrease in tumor score, despite having body

weight and lipid contents similar to WT mice (Figure 8B-C and Supplementary Figure S11). We found that active TGF- β 1 was not detectable in the plasma probably due to its short half-life of 2-3 min [55]. However, circulating total TGF- β 1 levels were significantly less in the DEN+HFD KO mice (Figure 8D). Serum levels of *LGALS3BP* were positively correlated with tumor scores (Figure 8E), and *TGFBI* and *LGALS3BP* expression was correlated positively in the liver tumors of WT mice (Figure 8F). Furthermore, the accumulation of collagen and α -SMA around the tumor nodules decreased in the KO mouse livers (Figure 8G). Levels of *TGFBI* and its associated genes were decreased in *LGALS3BP*-KO mouse liver tumors (Figure 8H-I). TGF- β 1-stained area near the tumor sites, JunB-positive nuclei, and the proliferation of tumor cells were all decreased (Figure 8J). *LGALS3BP* was required for the expression of *TGFBI* and its target genes, including *JUNB*, *PDGFB*, *VCAM1*, *SERPINE1*, and *COL1A1* in various HCC cell lines (Supplementary Figure S12).

4 | DISCUSSION

LGALS3BP and TGF- β 1 are crucial components of the innate immune response, and impairments in their function have been associated with organ fibrosis and the development of multiple tumors [5, 13, 25, 39]. By conducting an unbiased transcriptome analysis coupled with proteomics analysis and in vivo experiments using mouse models, we found that *LGALS3BP* plays a key role in regulating TGF- β 1 expression. Specifically, we uncovered mechanisms related to *LGALS3BP* that enhance the availability of TGF- β 1, which is crucial for controlling the acute immune environment and explains the persistence of inflammation-mediated organ fibrosis and carcinogenesis. As a tumor expands, fibroblasts close to cancer cells including cancer-associated fibroblasts (CAFs) often grow

treatment for 1h. Quantification of total stained area of p-FAK and the length of elongated filamentous actin from the p-FAK loci were shown on the left with five scanned images per slides of three independent experiments. Total numbers of F-actin used in the measurement were $n = 54$, $n = 120$, $n = 67$, and $n = 69$ from the left column. Data represented as mean \pm SD, *** $P < 0.001$ (Two-way ANOVA). (B) qRT-PCR analyses to measure the expression levels of *JUNB* and *TGFBI* in Hepa-1c1c7 cells upon r*LGALS3BP* \pm GLPG0187 treatment. Data represented as mean \pm SD, ** $P < 0.01$ and *** $P < 0.001$ (Two-way ANOVA). (C) Western blottings to detect the expression levels of indicated proteins. Quantification of the band intensities were shown on the left. Data represented as mean \pm SD, $n = 3$. *** $P < 0.001$ (Two-way ANOVA). (D) Immunofluorescence staining of phosphorylated FAK and F-actin in SNU449 cells upon r*LGALS3BP* \pm GLPG0187 treatment for 1h. Quantification of total stained area of p-FAK and the length of elongated filamentous actin from the p-FAK loci were shown on the left with five scanned images per slides of three independent experiments. Total numbers of F-actin used in the measurement were $n = 41$, $n = 80$, $n = 30$, and $n = 35$ from the left column. Data represented as mean \pm SD, *** $P < 0.001$ (Two-way ANOVA). (E) qRT-PCR analyses to measure the expression levels of *JUNB* and *TGFBI* in SNU449 cells upon r*LGALS3BP* \pm GLPG0187 treatment. Data represented as mean \pm SD, * $P < 0.05$, ** $P < 0.01$, and *** $P < 0.001$ (Two-way ANOVA). (F) Western blots to detect the expression levels of indicated proteins. Quantification of the band intensities were shown on the left. Data represented as mean \pm SD, $n = 3$. * $P < 0.05$, ** $P < 0.01$, and *** $P < 0.001$ (Two-way ANOVA). Abbreviations: DAPI, 4',6-diamidino-2-phenylindole; F-actin, filamentous actin; F-actin, filamentous actin; ITG α V, integrin subunit alpha V; p-FAK, phosphorylated focal adhesion kinase; r*LGALS3BP*, recombinant *LGALS3BP*; *TGFBI*, transforming growth factor beta 1.



along with the tumor and suppress immune surveillance. In such instances, an increased level of LGALS3BP in tumor cells can promote the growth of CAFs by increasing the availability of TGF- β 1. The high levels of TGF- β 1, as an essential regulator of innate immunity, can suppress the activity of natural killer cells, macrophages, and neutrophils, thereby creating an environment of negative immune regulation [24, 25]. We hypothesize that this may contribute to the oncogenic effects observed in patients with HCC who have elevated LGALS3BP levels.

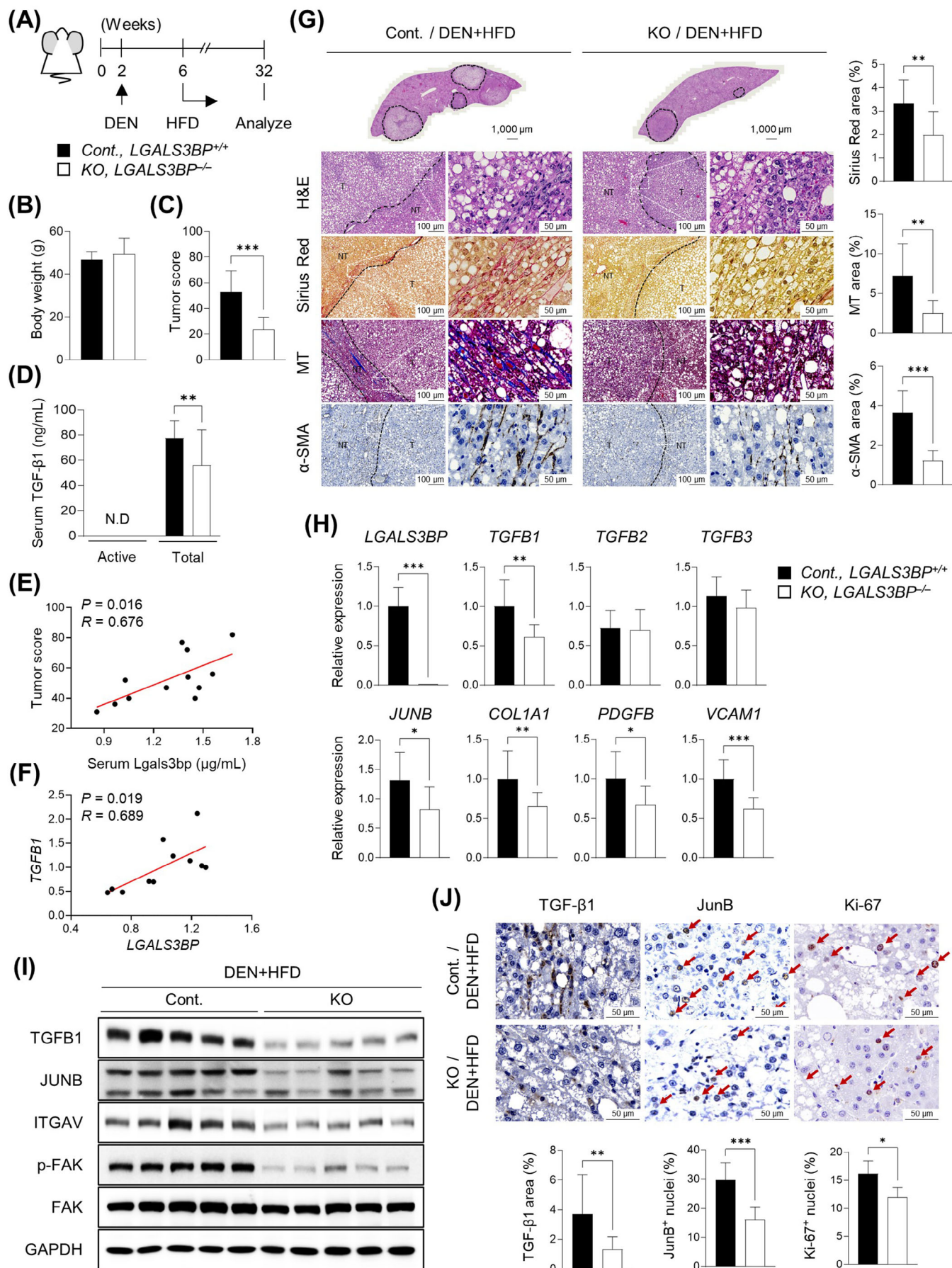
Serological and histological levels of LGALS3BP are significantly elevated in patients with hepatic fibrosis, cirrhosis, and HCC, and a correlation exists between increased LGALS3BP levels and the progression and aggravation of liver disease following viral infection. Assessing LGALS3BP levels is a non-invasive approach to disease diagnosis [16, 20, 22, 23, 56]. LGALS3BP levels are elevated in serum samples of patients with fibrosis or sepsis, in the secretome of human cerebral organoids, and in late-stage human fibrotic tissues; it is also commonly induced in tissues obtained from mouse models following liver injury induced by various pathological conditions such as concanavalin A or CCl₄ treatment, or common bile duct ligation [57–59]. Given that these investigations have focused on the role of LGALS3BP in the development of tissue fibrogenesis, further analyses (i.e., a more thorough assessment involving the IFN- α /LGALS3BP/TGF- β 1 axis, comprehensive serological analysis, and examination of secreted proteins through proteomic studies) should be performed to enable a more accurate diagnosis.

The development of hepatic fibrosis and carcinogenesis is influenced by numerous cells in the liver, such as hepatic stellate cells and Kupffer cells. When we analyzed the secreted levels of LGALS3BP in different cell types, NIH3T3, a fibroblast cell line, and RAW264.7, a macrophage cell line that could represent various cell types in the liver, including stellate and Kupffer cells. We found that the levels of secreted LGALS3BP were detectable in all cell types in serum-free culture medium.

Notably, the basal secretion level of LGALS3BP was the highest among the tested cell lines in RAW264.7. However, when the cells were exposed to 50U/ml IFN- α , the secreted LGALS3BP levels of Hepa-1c1c7 cells drastically increased compared to the subtle changes of RAW264.7 cells (Supplementary Figure S13). This suggests that hepatocytes are not the sole source of extracellular LGALS3BP and that in vivo levels are influenced by multiple factors in the environment. During physiological conditions, the initial increased secretion of LGALS3BP by epithelial hepatocytes, triggered by viral infections or toxic chemical-induced cell death, may be the primary source of extracellular LGALS3BP. However, quiescent stellate cells transformed into fibroblasts and infiltrated macrophages could be significant sources of extracellular LGALS3BP in pathological inflammation conditions.

ITG α V, in combination with the β 1, β 3, β 5, β 6, and β 8 integrins, forms heterodimeric receptors that bind to Arg-Gly-Asp and activate TGF- β 1 and TGF- β 3, which are key mediators of fibrosis [60]. TGF- β activation in latent complexes with myofibroblasts or epithelial cell integrins α v β 1, α v β 3, α v β 5, or α v β 6 requires cytoskeletal contractions when fibroblasts differentiate into myofibroblasts during fibrotic-tissue development or TGF- β 1-signaling activation in epithelial cells [50, 61, 62]. The initial activation of TGF- β 1 by LGALS3BP can trigger a feedforward loop involving the release of active TGF- β 1 (which upregulates *TGFBI*), leading to further upregulation of ECM-related proteins. These increased ECM marker levels result in a self-sustaining TGF- β 1-signaling condition since the necessary molecules (including the TGF- β 1 complex and its cognate receptor) are present in close proximity [29]. Investigations into the clinical use of small-molecule inhibitors targeting ITG α V, such as GLPG0187, have been used to treat various fibrosis-related diseases, including idiopathic pulmonary fibrosis, MASH, and coronavirus disease 2019 [46, 47, 62]. Given that ITG α V and TGF- β 1 play critical roles in various biological pathways, inhibition of these signaling axes by blocking LGALS3BP could be used to treat

FIGURE 7 Downregulation of TGF- β 1 signaling and CCl₄-induced fibrosis by *LGALS3BP* depletion. (A) Volcano plots of DEGs of the primary hepatocytes from *LGALS3BP*-KO mice compared with its control littermates ($n = 3$). (B) Pathway analyses of the upregulated genes. (C) Pathway analyses of the downregulated genes. (D) Experimental outline of the mouse model of hepatic fibrosis; *LGALS3BP*^{+/+} or *LGALS3BP*^{-/-} mice were intraperitoneally injected with CCl₄ twice per week for 6 weeks. All the mice were euthanized at 15 weeks of age. (E) qRT-PCR analysis of the indicated genes in the liver tissues. Data represented as mean \pm SD, $n = 6$ (vehicle injected groups) or $n = 7$ (CCl₄ injected groups). * $P < 0.05$, ** $P < 0.01$ and *** $P < 0.001$ (Two-way ANOVA). (F) Representative images of H&E, Sirius Red, MT staining, immunohistochemical staining of α -SMA or TGF- β 1 in the liver tissues. Quantification of the positively stained area were shown below. The stained areas were shown as percentages of the total area of each liver sections. Data represented as mean \pm SD, $n = 4-9$. * $P < 0.05$, ** $P < 0.01$, and *** $P < 0.001$ (Two-way ANOVA). (G) Representative TGF- β 1 western blotting of each group. Quantification of the band intensities were shown on the left. Data represented as mean \pm SD, $n = 3$. * $P < 0.05$, ** $P < 0.01$ and *** $P < 0.001$ (Two-way ANOVA). Abbreviations: *COL1A1*, collagen type I alpha 1; Cont., control; DEG, differentially expressed genes; H&E, hematoxylin and eosin stain; KO, knockout; *LGALS3BP*, lectin galactoside-binding soluble 3 binding protein; MT, Masson's trichrome stain; *TGFBI*, transforming growth factor beta 1; α -SMA, alpha-smooth muscle actin.



several diseases, including those associated with fibrosis and carcinogenesis.

Further comprehensive studies are required on the interacting domains/motifs and the requirement of LGALS3BP glycosylation for interactions between LGALS3BP and ITGs to develop tools for enhancing or blocking rigid actin cytoskeleton formation. Another route by which ITG α V is activated involves the enhanced arrangement of its ligands around cells by LGALS3BP. Fibronectin, an ECM protein that interacted with LGALS3BP (Figure 5C), mediates cell-to-ECM interactions during wound healing, fibrosis, and tumor progression, and functions as a ligand for ITG α V [11, 63]. Therefore, it is imperative to elucidate the related physical interactions at the molecular level to facilitate the development of drugs to cure diseases caused by aberrant TGF- β 1 signaling.

The persistent viral infections caused by HBV or HCV led to chronic inflammation, which is a key factor in the progression of MASH [64, 65]. LGALS3BP plays a substantial role in the body's defense mechanism and has been shown to have antiviral activity against a range of viral infections, such as influenza A virus, vesicular stomatitis virus, and herpes simplex virus, according to previous studies [4]. This suggests that LGALS3BP likely plays a role in regulating MASH symptoms caused by viral infections. However, while the function of LGALS3BP in the context of infectious diseases has been relatively well-investigated, its role in sterile inflammation, including chemical-induced hepatic fibrosis and metabolic dysfunction associated steatohepatitis, has received less attention in research. Our aim was to explore the role of

LGALS3BP in a sterile inflammation context where there was no detectable viral load. Our results indicated that LGALS3BP was markedly induced in these situations, such as in response to CCl₄ injection, a high-fat methionine-choline-deficient diet, or a DEN-high fat diet. Our study emphasized the critical role of LGALS3BP in regulating the fibrogenic TGF- β 1 signaling pathway in sterile inflammation. We hypothesize that LGALS3BP may have a similar role in infectious diseases and metabolic dysfunction by regulating TGF- β 1, but the role of LGALS3BP-TGF- β 1 axis in infectious diseases needs to be validated in future studies.

5 | CONCLUSIONS

LGALS3BP secretion is a key factor that initiates TGF- β 1 signaling, which is crucial for regulating inflammatory responses, fibrosis, and carcinogenesis in the liver. This finding provides a better understanding of the molecular mechanisms underlying these processes and could lead to the development of effective therapies for malignant tumors.

AUTHOR CONTRIBUTIONS

DHK and MS conceptualized the study and drafted the manuscript. DHK, MS, MSP, KR, EGS, KHY, and SYJ designed experiments and developed the methodology. DHK, MS, MSP and KR performed the cell line and mouse model experiments. SYJ analyzed the human MASH patients' data. SYJ performed and analyzed the LC-MS/MS proteomics study. WKB, SHC, and IJC interpreted data

FIGURE 8 Reduction of the steatohepatitis-induced hepatocarcinogenesis by *LGALS3BP* depletion. (A) Experimental outline of the HCC mouse model. *LGALS3BP*^{+/+} and *LGALS3BP*^{-/-} mice were injected intraperitoneally with 25 mg/kg DEN at 2 weeks after birth and fed an HFD for 26 weeks beginning at 6 weeks of age. All the mice were euthanized at 32 weeks of age. (B) Body weights of control and *LGALS3BP*-KO mice on the day of euthanasia ($n = 12-13$). (C) Tumor scores of the control and KO mouse livers. Tumors ≤ 5 mm were assigned a value of 1 and tumors > 5 mm were multiplied by 2. Tumor scores were determined as the sum of the values. Data represented as mean \pm SD, $n = 12-13$. *** $P < 0.001$ (Student's t -test). (D) ELISA assays for the measurement of active or total TGF- β 1 levels in the serum at the time of the sacrifice. Data represented as mean \pm SD, $n = 12-13$. ** $P < 0.01$ (Student's t -test). (E) The correlation between the tumor score and serum *LGALS3BP* levels in the control mice ($n = 12$). (F) The correlation between the *TGFBI* and *LGALS3BP* in the tumor tissues of control mice. (G) Upper panels: whole tumor-bearing mouse livers and its H&E-stained sections; lower panels: liver sections stained with H&E, Sirius Red, MT, and α -SMA IHC. Quantification of the positive stained areas were shown on the left. The stained areas were shown as percentages of the total area of each liver sections. Data represented as mean \pm SD, $n = 10-12$. ** $P < 0.01$ and *** $P < 0.001$ (Student's t -test). (H) qRT-PCR analysis of the indicated genes in hepatic tumors isolated from control and *LGALS3BP*-KO mice. Data represented as mean \pm SD, $n = 10-12$. * $P < 0.05$, ** $P < 0.01$ and *** $P < 0.001$ (Student's t -test). (I) Representative western blottings to detect the expressions of indicated proteins in the cont. and KO mice liver tissues. (J) Representative immunohistochemical staining of TGF- β 1, JunB, and Ki-67 in the indicated mouse liver tissues. Quantification of the positively stained area were shown below. The stained areas were shown as percentages of the total area of each liver sections. Data represented as mean \pm SD, $n = 16-17$ for TGF- β 1, $n = 10-11$ for JunB and Ki-67. * $P < 0.05$, ** $P < 0.01$, and *** $P < 0.001$ (Student's t -test). Abbreviations: *COL1A1*, collagen type I alpha 1; Cont., control; DEN, diethylnitrosamine; GAPDH, glyceraldehyde 3-phosphate dehydrogenase; H&E, hematoxylin and eosin stain; H&E, hematoxylin and eosin stain; HFD, high fat diet; ITG α V, integrin subunit alpha V; KO, knockout; *LGALS3BP*, lectin galactoside-binding soluble 3 binding protein; MT, Masson's trichrome stain; MT, Masson's trichrome stain; *PDGFB*, platelet derived growth factor subunit B; p-FAK, phosphorylated focal adhesion kinase; SMA, alpha-smooth muscle actin; *TGFBI*, transforming growth factor beta 1; *VCAMI*, vascular cell adhesion protein 1; α -SMA, alpha-smooth muscle actin.

and reviewed the manuscript. All authors have read and approved the final manuscript.

ACKNOWLEDGMENTS

The biospecimens and data used in this study were provided by the Biobank of Chonnam National University Hwasun Hospital, a member of the Korea Biobank Network. This research was supported by the Bio & Medical Technology Development Program of the National Research Foundation (NRF) (grant number NRF-2020M3A9G3080281) and an NRF grant (grant number NRF-2020R1A5A2031185) funded by the Korean Government.

CONFLICTS OF INTEREST STATEMENTS

None.



DATA AVAILABILITY STATEMENT

RNA-seq and ATAC-seq data generated in this study were deposited in the GEO database under the accession codes GSE271352, GSE271354, and GSE271355, including all raw and processed data.

ETHICS APPROVAL STATEMENT AND CONSENT TO PARTICIPATE

This study was approved by the Chonnam National University Hwasun Hospital Ethics Committee (approval number: IRB CNUHH-2021-187). Written informed consent for participation was obtained from all the patients.

ORCID

Kyung Hyun Yoo  <https://orcid.org/0000-0003-2172-5564>
Ik-Joo Chung  <https://orcid.org/0000-0003-0479-8067>

REFERENCES

- Llovet JM, Kelley RK, Villanueva A, Singal AG, Pikarsky E, Roayaie S, et al. Hepatocellular carcinoma. *Nat Rev Dis Primers*. 2021;7(1):6.
- Ringelhan M, Pfister D, O'Connor T, Pikarsky E, Heikenwalder M. The immunology of hepatocellular carcinoma. *Nat Immunol*. 2018;19(3):222–232.
- Craig AJ, von Felden J, Garcia-Lezana T, Sarcognato S, Villanueva A. Tumour evolution in hepatocellular carcinoma. *Nat Rev Gastroenterol Hepatol*. 2020;17(3):139–152.
- Xu G, Xia Z, Deng F, Liu L, Wang Q, Yu Y, et al. Inducible LGALS3BP/90K activates antiviral innate immune responses by targeting TRAF6 and TRAF3 complex. *PLoS Pathog*. 2019;15(8):e1008002.
- Loimaranta V, Hepojoki J, Laaksoaho O, Pulliainen AT. Galectin-3-binding protein: A multitask glycoprotein with innate immunity functions in viral and bacterial infections. *J Leukoc Biol*. 2018;104(4):777–786.
- Laubli H, Alisson-Silva F, Stanczak MA, Siddiqui SS, Deng L, Verhagen A, et al. Lectin galactoside-binding soluble 3 binding protein (LGALS3BP) is a tumor-associated immunomodulatory ligand for CD33-related Siglecs. *J Biol Chem*. 2014;289(48):33481–33491.
- Kono M, Nakamura Y, Oyama Y, Mori K, Hozumi H, Karayama M, et al. Increased levels of serum Wisteria floribunda agglutinin-positive Mac-2 binding protein in idiopathic pulmonary fibrosis. *Respir Med*. 2016;115:46–52.
- Alkhouiri N, Johnson C, Adams L, Kitajima S, Tsuruno C, Colpitts TL, et al. Serum Wisteria floribunda agglutinin-positive Mac-2-binding protein levels predict the presence of fibrotic nonalcoholic steatohepatitis (NASH) and NASH cirrhosis. *PLoS One*. 2018;13(8):e0202226.
- Costa J, Pronto-Laborinho A, Pinto S, Gromicho M, Bonucci S, Tranfield E, et al. Investigating LGALS3BP/90 K glycoprotein in the cerebrospinal fluid of patients with neurological diseases. *Sci Rep*. 2020;10(1):5649.
- Iacobelli S, Natoli C, D'Egidio M, Tamburrini E, Antinori A, Ortona L. Lipoprotein 90K in human immunodeficiency virus-infected patients: a further serologic marker of progression. *J Infect Dis*. 1991;164(4):819.
- Piccolo E, Tinari N, Semeraro D, Traini S, Fichera I, Cumashi A, et al. LGALS3BP, lectin galactoside-binding soluble 3 binding protein, induces vascular endothelial growth factor in human breast cancer cells and promotes angiogenesis. *J Mol Med (Berl)*. 2013;91(1):83–94.
- Traini S, Piccolo E, Tinari N, Rossi C, La Sorda R, Spinella F, et al. Inhibition of tumor growth and angiogenesis by SP-2, an anti-lectin, galactoside-binding soluble 3 binding protein (LGALS3BP) antibody. *Mol Cancer Ther*. 2014;13(4):916–925.
- Capone E, Iacobelli S, Sala G. Role of galectin 3 binding protein in cancer progression: a potential novel therapeutic target. *J Transl Med*. 2021;19(1):405.
- Inoue T, Tanaka Y. Novel biomarkers for the management of chronic hepatitis B. *Clin Mol Hepatol*. 2020;26(3):261–279.
- Chuaypen N, Chittmitrarpap S, Pinjaroen N, Sirichindakul B, Poovorawan Y, Tanaka Y, et al. Serum Wisteria floribunda agglutinin-positive Mac-2 binding protein level as a diagnostic marker of hepatitis B virus-related hepatocellular carcinoma. *Hepatol Res*. 2018;48(11):872–881.
- Artini M, Natoli C, Tinari N, Costanzo A, Marinelli R, Balsano C, et al. Elevated serum levels of 90K/MAC-2 BP predict unresponsiveness to alpha-interferon therapy in chronic HCV hepatitis patients. *J Hepatol*. 1996;25(2):212–217.
- Kittl EM, Hofmann J, Hartmann G, Sebesta C, Beer F, Bauer K, et al. Serum protein 90K/Mac-2BP is an independent predictor of disease severity during hepatitis C virus infection. *Clin Chem Lab Med*. 2000;38(3):205–208.
- Gutmann C, Takov K, Burnap SA, Singh B, Ali H, Theofilatos K, et al. SARS-CoV-2 RNAemia and proteomic trajectories inform prognostication in COVID-19 patients admitted to intensive care. *Nat Commun*. 2021;12(1):3406.
- Tawara S, Tatsumi T, Iio S, Kobayashi I, Shigekawa M, Hikita H, et al. Evaluation of Fucosylated Haptoglobin and Mac-2 Binding Protein as Serum Biomarkers to Estimate Liver Fibrosis in Patients with Chronic Hepatitis C. *PLoS One*. 2016;11(3):e0151828.
- Kuno A, Ikehara Y, Tanaka Y, Ito K, Matsuda A, Sekiya S, et al. A serum "sweet-doughnut" protein facilitates fibrosis evaluation and therapy assessment in patients with viral hepatitis. *Sci Rep*. 2013;3:1065.

21. Saleh SA, Salama MM, Alhusseini MM, Mohamed GA. M2BPGi for assessing liver fibrosis in patients with hepatitis C treated with direct-acting antivirals. *World J Gastroenterol*. 2020;26(21):2864–2876.
22. Iacovazzi PA, Trisolini A, Barletta D, Elba S, Manghisi OG, Correale M. Serum 90K/MAC-2BP glycoprotein in patients with liver cirrhosis and hepatocellular carcinoma: a comparison with alpha-fetoprotein. *Clin Chem Lab Med*. 2001;39(10):961–965.
23. Correale M, Giannuzzi V, Iacovazzi PA, Valenza MA, Lanzillotta S, Abbate I, et al. Serum 90K/MAC-2BP glycoprotein levels in hepatocellular carcinoma and cirrhosis. *Anticancer Res*. 1999;19(4C):3469–3472.
24. Derynck R, Turley SJ, Akhurst RJ. TGFbeta biology in cancer progression and immunotherapy. *Nat Rev Clin Oncol*. 2021;18(1):9–34.
25. Peng D, Fu M, Wang M, Wei Y, Wei X. Targeting TGF-beta signal transduction for fibrosis and cancer therapy. *Mol Cancer*. 2022;21(1):104.
26. Meng XM, Nikolic-Paterson DJ, Lan HY. TGF-beta: the master regulator of fibrosis. *Nat Rev Nephrol*. 2016;12(6):325–338.
27. Pickup M, Novitskiy S, Moses HL. The roles of TGFbeta in the tumour microenvironment. *Nat Rev Cancer*. 2013;13(11):788–799.
28. Munger JS, Huang X, Kawakatsu H, Griffiths MJ, Dalton SL, Wu J, et al. The integrin alpha v beta 6 binds and activates latent TGF beta 1: a mechanism for regulating pulmonary inflammation and fibrosis. *Cell*. 1999;96(3):319–328.
29. Wipff PJ, Hinz B. Integrins and the activation of latent transforming growth factor beta1 - an intimate relationship. *Eur J Cell Biol*. 2008;87(8-9):601–615.
30. Robertson IB, Rifkin DB. Regulation of the Bioavailability of TGF-beta and TGF-beta-Related Proteins. *Cold Spring Harb Perspect Biol*. 2016;8(6):a021907.
31. Hong CS, Park MR, Sun EG, Choi W, Hwang JE, Bae WK, et al. Gal-3BP Negatively Regulates NF-kappaB Signaling by Inhibiting the Activation of TAK1. *Front Immunol*. 2019;10:1760.
32. Uehara T, Pogribny IP, Rusyn I. The DEN and CCl(4) - Induced Mouse Model of Fibrosis and Inflammation-Associated Hepatocellular Carcinoma. *Curr Protoc*. 2021;1(8):e211.
33. Fujii T, Fuchs BC, Yamada S, Lauwers GY, Kulu Y, Goodwin JM, et al. Mouse model of carbon tetrachloride induced liver fibrosis: Histopathological changes and expression of CD133 and epidermal growth factor. *BMC Gastroenterol*. 2010;10:79.
34. Park EJ, Lee JH, Yu GY, He G, Ali SR, Holzer RG, et al. Dietary and genetic obesity promote liver inflammation and tumorigenesis by enhancing IL-6 and TNF expression. *Cell*. 2010;140(2):197–208.
35. Xie Z, Bailey A, Kuleshov MV, Clarke DJB, Evangelista JE, Jenkins SL, et al. Gene Set Knowledge Discovery with Enrichr. *Curr Protoc*. 2021;1(3):e90.
36. Heinz S, Benner C, Spann N, Bertolino E, Lin YC, Laslo P, et al. Simple combinations of lineage-determining transcription factors prime cis-regulatory elements required for macrophage and B cell identities. *Mol Cell*. 2010;38(4):576–589.
37. Gomes LR, Terra LF, Wailemann RA, Labriola L, Sogayar MC. TGF-beta1 modulates the homeostasis between MMPs and MMP inhibitors through p38 MAPK and ERK1/2 in highly invasive breast cancer cells. *BMC Cancer*. 2012;12:26.
38. Santibanez JF, Obradovic H, Kukolj T, Krstic J. Transforming growth factor-beta, matrix metalloproteinases, and urokinase-type plasminogen activator interaction in the cancer epithelial to mesenchymal transition. *Dev Dyn*. 2018;247(3):382–395.
39. Deng Z, Fan T, Xiao C, Tian H, Zheng Y, Li C, et al. TGF-beta signaling in health, disease, and therapeutics. *Signal Transduct Target Ther*. 2024;9(1):61.
40. Alvarez MD, Ronco MT, Ochoa JE, Monti JA, Carnovale CE, Pisani GB, et al. Interferon alpha-induced apoptosis on rat preneoplastic liver is mediated by hepatocytic transforming growth factor beta. *Hepatology*. 2004;40(2):394–402.
41. Alvarez Mde L, Quiroga AD, Parody JP, Ronco MT, Frances DE, Carnovale CE, et al. Cross-talk between IFN-alpha and TGF-beta1 signaling pathways in preneoplastic rat liver. *Growth Factors*. 2009;27(1):1–11.
42. Jonk LJ, Itoh S, Heldin CH, ten Dijke P, Kruijer W. Identification and functional characterization of a Smad binding element (SBE) in the JunB promoter that acts as a transforming growth factor-beta, activin, and bone morphogenetic protein-inducible enhancer. *J Biol Chem*. 1998;273(33):21145–21152.
43. Sundqvist A, Morikawa M, Ren J, Vasilaki E, Kawasaki N, Kobayashi M, et al. JUNB governs a feed-forward network of TGFbeta signaling that aggravates breast cancer invasion. *Nucleic Acids Res*. 2018;46(3):1180–1195.
44. Hariyanto NI, Yo EC, Wanandi SI. Regulation and Signaling of TGF-beta Autoinduction. *Int J Mol Cell Med*. 2021;10(4):234–247.
45. Zhang Y, Feng XH, Derynck R. Smad3 and Smad4 cooperate with c-Jun/c-Fos to mediate TGF-beta-induced transcription. *Nature*. 1998;394(6696):909–913.
46. Cirkel GA, Kerklaan BM, Vanhoutte F, Van der Aa A, Lorenzon G, Namour F, et al. A dose escalating phase I study of GLPG0187, a broad spectrum integrin receptor antagonist, in adult patients with progressive high-grade glioma and other advanced solid malignancies. *Invest New Drugs*. 2016;34(2):184–192.
47. Huntington KE, Carlsen L, So EY, Piesche M, Liang O, El-Deiry WS. Integrin/TGF-beta1 Inhibitor GLPG-0187 Blocks SARS-CoV-2 Delta and Omicron Pseudovirus Infection of Airway Epithelial Cells In Vitro, Which Could Attenuate Disease Severity. *Pharmaceuticals (Basel)*. 2022;15(5):618.
48. Olson EN, Nordheim A. Linking actin dynamics and gene transcription to drive cellular motile functions. *Nat Rev Mol Cell Biol*. 2010;11(5):353–365.
49. Pang X, He X, Qiu Z, Zhang H, Xie R, Liu Z, et al. Targeting integrin pathways: mechanisms and advances in therapy. *Signal Transduct Target Ther*. 2023;8(1):1.
50. Dong X, Zhao B, Iacob RE, Zhu J, Koksai AC, Lu C, et al. Force interacts with macromolecular structure in activation of TGF-beta. *Nature*. 2017;542(7639):55–59.
51. Grassadonia A, Graziano V, Pagotto S, Veronese A, Giuliani C, Marchisio M, et al. Tgf-beta1 transcriptionally promotes 90K expression: possible implications for cancer progression. *Cell Death Discov*. 2021;7(1):86.
52. Govaere O, Cockell S, Tiniakos D, Queen R, Younes R, Vacca M, et al. Transcriptomic profiling across the nonalcoholic fatty liver disease spectrum reveals gene signatures for steatohepatitis and fibrosis. *Sci Transl Med*. 2020;12(572):eaba4448.
53. Ikawa-Yoshida A, Matsuo S, Kato A, Ohmori Y, Higashida A, Kaneko E, et al. Hepatocellular carcinoma in a mouse model fed a choline-deficient, L-amino acid-defined, high-fat diet. *Int J Exp Pathol*. 2017;98(4):221–233.

54. Tokinoya K, Sekine N, Aoki K, Ono S, Kuji T, Sugawara T, et al. Effects of renalase deficiency on liver fibrosis markers in a nonalcoholic steatohepatitis mouse model. *Mol Med Rep.* 2021;23(3):210.
55. Coffey RJ, Jr., Kost LJ, Lyons RM, Moses HL, LaRusso NF. Hepatic processing of transforming growth factor beta in the rat. Uptake, metabolism, and biliary excretion. *J Clin Invest.* 1987;80(3):750–757.
56. Cheung KJ, Libbrecht L, Tilleman K, Deforce D, Colle I, Van Vlierberghe H. Galectin-3-binding protein: a serological and histological assessment in accordance with hepatitis C-related liver fibrosis. *Eur J Gastroenterol Hepatol.* 2010;22(9):1066–1073.
57. Yang B, Zhang J, Sun L, Huang T, Kong Y, Li L, et al. Mapping Novel Biomarkers of Liver Injury by Tissue Proteomic Analysis. *ACS Omega.* 2021;6(10):7127–7138.
58. Baker ES, Burnum-Johnson KE, Jacobs JM, Diamond DL, Brown RN, Ibrahim YM, et al. Advancing the high throughput identification of liver fibrosis protein signatures using multiplexed ion mobility spectrometry. *Mol Cell Proteomics.* 2014;13(4):1119–1127.
59. Luo M, Zhang Q, Hu Y, Sun C, Sheng Y, Deng C. LGALS3BP: A Potential Plasma Biomarker Associated with Diagnosis and Prognosis in Patients with Sepsis. *Infect Drug Resist.* 2021;14:2863–2871.
60. Margadant C, Sonnenberg A. Integrin-TGF-beta crosstalk in fibrosis, cancer and wound healing. *EMBO Rep.* 2010;11(2):97–105.
61. Conroy KP, Kitto LJ, Henderson NC. alphav integrins: key regulators of tissue fibrosis. *Cell Tissue Res.* 2016;365(3):511–519.
62. Slack RJ, Macdonald SJF, Roper JA, Jenkins RG, Hatley RJD. Emerging therapeutic opportunities for integrin inhibitors. *Nat Rev Drug Discov.* 2022;21(1):60–78.
63. Huang J, Zhang L, Wan D, Zhou L, Zheng S, Lin S, et al. Extracellular matrix and its therapeutic potential for cancer treatment. *Signal Transduct Target Ther.* 2021;6(1):153.
64. Hannah WN, Jr., Torres DM, Harrison SA. Nonalcoholic Steatohepatitis and Endpoints in Clinical Trials. *Gastroenterol Hepatol (N Y).* 2016;12(12):756–763.
65. Tian Z, Xu C, Yang P, Lin Z, Wu W, Zhang W, et al. Molecular pathogenesis: Connections between viral hepatitis-induced and non-alcoholic steatohepatitis-induced hepatocellular carcinoma. *Front Immunol.* 2022;13:984728.

SUPPORTING INFORMATION

Additional supporting information can be found online in the Supporting Information section at the end of this article.

How to cite this article: Kim D-H, Sung M, Park M-S, Sun E-G, Yoon S, Yoo KH, et al. Galectin 3-binding protein (LGALS3BP) depletion attenuates hepatic fibrosis by reducing transforming growth factor- β 1 (TGF- β 1) availability and inhibits hepatocarcinogenesis. *Cancer Commun.* 2024;44:1106–1129.
<https://doi.org/10.1002/cac2.12600>